Progress in Aerospace Sciences 45 (2009) 124–146

Contents lists available at ScienceDirect

Progress in Aerospace Sciences

journal homepage: www.elsevier.com/locate/paerosci

Supersonic drag reduction technology in the scaled supersonic experimental airplane project by JAXA

Kenji Yoshida *

Aviation Program Group, Japan Aerospace Exploration Agency (JAXA), 6-13-1 Osawa, Mitaka, Tokyo 181-0015, Japan

ARTICLE INFO

Available online 8 August 2009

ABSTRACT

Anticipating the international cooperative development of a next generation supersonic transport (SST), Japan Aerospace Exploration Agency (JAXA) has developed an advanced drag reduction technique as one of the key technologies that will be required. JAXA's technique is based on an aerodynamically optimum combination of well-known pressure drag reduction concepts and a new friction drag reduction concept. The pressure drag reduction concepts are mainly grounded in supersonic linear theory and involve the application of an arrow planform, a warped wing with optimum camber and twist, and an area-ruled body. The friction drag reduction concept is a world-first technical approach that obtains a natural laminar flow wing with a subsonic leading edge at supersonic speed. An ideal pressure distribution is first designed to delay boundary layer transition even on a highly swept wing, then an original CFD-based inverse design method is applied to obtain a wing shape that realizes the pressure distribution. An unmanned and scaled supersonic experimental airplane was flown at the Woomera test field in Australia in October 2005 to prove those concepts. Flight data analysis and comparison of flight data with CFD design data validated the drag reduction technique both qualitatively and quantitatively.

Contents

* Tel.: +81 422 40 3500; fax: +81 422 40 3536.
E-mail address: yoshida.kenji@jaxa.jp

0376-0421/$ - see front matter © 2009 Elsevier Ltd. All rights reserved.
doi:10.1016/j.paerosci.2009.05.002

1. Introduction

Innovative advanced technologies will be necessary to develop a next generation supersonic transport (SST) that has excellent economic and environmental characteristics. From an economic standpoint, challenges include improving the lift-to-drag ratio in supersonic cruise and the low-speed aerodynamic performance. From an environmental standpoint, it is required to minimize the sonic boom generated when the aircraft flies supersonically, reduce NOx and CO_2 emissions from the propulsion system, and reduce the noise due to propulsion system and airframe during takeoff and landing. Following the development of the Concorde, a number of research efforts have been made around the world towards these goals, and research in these challenging areas should be also promoted in Japan because developing a next generation SST will require international collaboration.

Japan Aerospace Exploration Agency (JAXA) has been promoting development of several technologies that will be required for a next generation SST. The National EXperimental Supersonic Transport (NEXST) program [1,2] was carried out from 1997 to 2006, and a follow-on program, the Silent SuperSonic Technology Demonstrator (S3TD) [3] has been planned. In the NEXST program, several computational fluid dynamics (CFD)-based aerodynamic design techniques were developed for reducing aerodynamic drag at supersonic speed, optimizing high-lift devices for takeoff and landing, and creating a new sonic boom reduction concept as shown in Fig. 1.

Particularly for the development of supersonic drag reduction techniques, flight test validation was planned using two experimental vehicles. One vehicle, the "Non-powered experimental airplane" or "NEXST-1 airplane", is a purely aerodynamic configuration for validating JAXA's innovative drag reduction concepts.

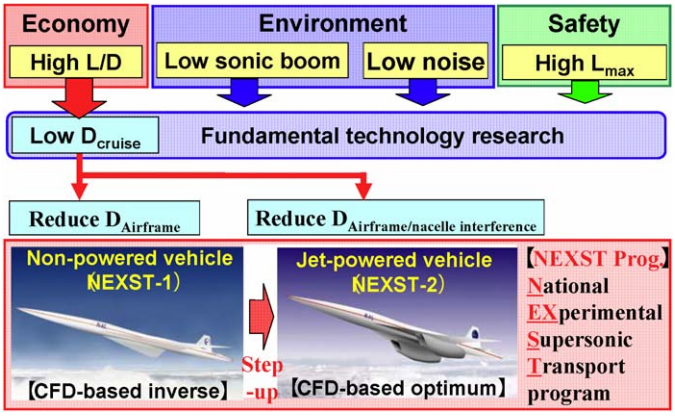

Fig. 1. Structure of the unmanned-scaled supersonic experimental vehicle program of JAXA.

This is launched and inserted into the flight test conditions by a solid rocket booster. The other vehicle, simply called the "Jet-powered airplane" or "NEXST-2 airplane", has an aerodynamically designed configuration and a jet propulsion system for validating the airframe–propulsion interference drag reduction concept.

The NEXST-1 airplane was developed first. A CFD-based inverse design method incorporating well-known pressure drag reduction concepts and an original friction drag reduction concept was developed and applied to its aerodynamic design. Present pressure drag reduction concepts are a suitable wing planform, an optimally cambered and twisted wing, and an area-ruled body. The friction drag reduction concept is based on a supersonic natural laminar flow wing design, which was derived in the case of an SST with subsonic leading edge as a first challenge in the world.

The NEXST-2 airplane was next to be developed using a CFD-based aerodynamic optimum design method incorporating both the NEXST-1 design concepts and an original non-axisymmetrical area-ruled body design concept to reduce interference drag between the airframe and two engine nacelles. The CFD-based optimum design method consists of Euler analysis with an overset grid system and application of the adjoint technique for sensitivity analysis of design variables.

The first flight test of NEXST-1 was conducted on 14 July 2002, but failed because of premature separation of the booster due to an electrical short in the firing system of separation bolts. This resulted in the freezing and ultimate cancellation of NEXST-2 project, and all efforts were poured into improving and redesigning the NEXST-1 airplane system for a second flight test. About 3 years later, on 10 October 2005, a second flight test was successfully conducted and much aerodynamic data were obtained. Through analyzing the flight data and comparing them with CFD-predicted aerodynamic characteristics, the NEXST-1 aerodynamic design technology was validated both qualitatively and quantitatively.

Presently, JAXA is engaged in a program to design a silent supersonic technology demonstrator (S3TD) in place of the cancelled NEXST-2 project. In this program, an optimum aerodynamic design technique incorporating multi-disciplinary optimization design (MDO) has been developed to reduce supersonic drag, sonic boom, weight penalty, and to improve low-speed performance. In particular, the S3TD is designed to reduce sonic boom by applying an original low-boom concept. A flight test campaign to validate the technology is also being investigated.

This paper chiefly presents the details of the NEXST-1 aerodynamic design technique, namely a CFD-based inverse design method for supersonic drag reduction. In addition, the airframe–nacelle interference drag reduction technique applied to the design of the NEXST-2 airplane and an optimum design method developed for the S3TD program are briefly described with reference to JAXA research reports.

In Section 2, the general characteristics of supersonic drag and a target level of drag reduction are first of all described as a background to the NEXST program. Then, several drag reduction concepts for a next generation SST are discussed and summarized. In Section 3, the NEXST-1 design techniques are presented in detail, including the aerodynamic design process, preliminary validation by wind tunnel tests, final validation by flight test data analysis, and a discussion of the practical application of the techniques to a full-sized SST. Finally, the NEXST-2 design and S3TD design techniques are summarized briefly in Section 4.

2. Supersonic drag reduction technology

2.1. Supersonic drag components

Precisely speaking, it is not easy to clearly identify all the sources of aerodynamic drag for a complete aircraft, which is typically a wing–body–tail configuration with a propulsion system and protuberances such as antennas, air data sensors and lights. However, drag can be analyzed approximately by breaking it down into three components as follows:

$$D(total) = D(airframe) + D(propulsion) + D(interference) \tag{1}$$

Here, airframe drag refers to the drag of a configuration without a propulsion system. Propulsion drag consists roughly of intake drag sources such as spillage, bleed, and bypass drag, and friction drag on nacelle surfaces. Interference drag is mainly generated by interference between the airframe and propulsion system, and also by miscellaneous drag sources. It is possible to estimate interference drag roughly using an empirical database and CFD to analyze interference regions.

A typical SST configuration consists of a slender fuselage, a thin wing, and horizontal/vertical tails and engine nacelles that are relatively small compared with the wing and fuselage dimensions. The main source of drag for an SST is therefore airframe drag in supersonic cruise. In this and the following sections, we mainly discuss design concepts and methods for reducing this airframe drag. Methods for reducing propulsion and interference drag are briefly mentioned later in this paper.

2.1.1. Drag breakdown

Aerodynamic drag generally consists of friction drag and pressure drag. Friction drag is determined almost entirely by the state of the boundary layer (laminar, transition or turbulent), and does not vary greatly between subsonic and supersonic flight. On the other hand, pressure drag increases markedly at supersonic speed due to shock waves generated by the airframe and propulsion system. The increased drag is called "wave drag".

Aerodynamic drag is also divided into zero-lift drag and lift-dependent drag components. In general, friction drag is treated approximately as zero-lift drag, because friction drag is not sensitive in the change of angle of attack, namely lift condition being satisfied with attached flow condition. Shock waves are produced by deflections of the flow by airframe volumes, such as the cross-sectional area distribution of the fuselage and the thickness distribution of the wing, and by lift generation. The former corresponds to zero-lift drag and is called "wave drag due to volume". The latter is lift-dependent drag called "wave drag due to lift". Furthermore, lift-dependent drag includes a component called "induced drag" at subsonic speed, which is generated by trailing vortices such as wing tip vortices.

These components of drag at supersonic speed are summarized in the form of drag coefficients as follows:

$$\begin{aligned} C_D(airframe) &= C_{Df}(friction) + C_{Dp}(pressure) \\ &= C_{Df}(friction) + C_{Dw}(wave) + C_{Dv}(vortex) \\ &= C_{Df}(friction) + C_{Dwv}(wave\ \ due\ \ to\ \ volume) \\ &\quad + C_{Dwl}(wave\ \ due\ \ to\ \ lift) + C_{Dv}(vortex) \\ &= C_{D0}(zero\ \ lift) + C_{Dl}(lift - dependent) \end{aligned} \tag{2}$$

where

$$\begin{aligned} &C_{Dp}(pressure) = C_{Dw}(wave) + C_{Dv}(vortex) \\ &C_{Dw}(wave) = C_{Dwv}(wave\ due\ to\ volume) + C_{Dwl}(wave\ due\ to\ lift) \\ &C_{D0}(zero\ lift) = C_{Df}(friction) + C_{Dwv}(wave\ due\ to\ volume) \\ &C_{Dl}(lift - dependent) = C_{Dwl}(wave\ due\ to\ lift) + C_{Dv}(vortex) \end{aligned} \tag{3}$$

2.1.2. Drag formulation

To predict drag characteristics in preliminary design studies of a next generation SST, it is necessary to have concrete, practical expressions to estimate each drag component. Japan Aircraft Development Corporation (JADC) and various Japanese airframe industries (JAI) such as Mitsubishi Heavy Industries (MHI), Kawasaki Heavy Industries (KHI) and Fuji Heavy Industries (FHI), investigated the drag characteristics of a next generation SST about 20 years ago [4,5], and as a result approximate formulations of each drag component were derived as detailed in Ref. [6].

2.1.2.1. Friction drag. Total friction drag is estimated by summing the friction drag of each part of an SST configuration. The same formulation shown below is used for the friction drag of all parts, but the reference length and wetted area of each part are different.

$$C_{Df} = C_f(Re_L, M)\frac{S_{wet}}{S_w}$$
$$\text{where}\quad C_f(Re_L, M) = C_{fi}(Re_L) f(M) \tag{4}$$

$$\begin{cases} C_{fi}(Re_L) = \dfrac{0.455}{(\log_{10} Re_L)^{2.58}}: \ \ Prandtl's\ \ formula \\ \qquad [incompressible\ \ friction\ \ coefficient] \\ f(M) = \left(1 + 0.15M^2\right)^{-0.58}: \ \ Hoerner's\ \ formula \\ \qquad [Mach\ \ number\ \ correction] \end{cases} \tag{5}$$

where S_w : *wing area*
$S_{wet,each}$: each wetted area on each component
Re_L : each Ryenolds number based on each reference length

The formulation for the incompressible skin friction coefficient assumes a turbulent boundary layer on a flat plate and no super-velocity effect. It is called Prandtl's formula and is principally dominated by the Reynolds number based on the reference length of each part of the SST configuration. The effect of Mach number on the skin friction coefficient is corrected by Hoerner's formula.

2.1.2.2. Wave drag due to volume. The formulations for wave drag due to volume are generally divided into two groups: one for wing type and another for the axisymmetric body type.

(i) Wing type
The formula for wing type is derived by introducing an empirical coefficient K_0 to the theoretical optimum solution for minimum wave drag due to volume by Sears and Haack.

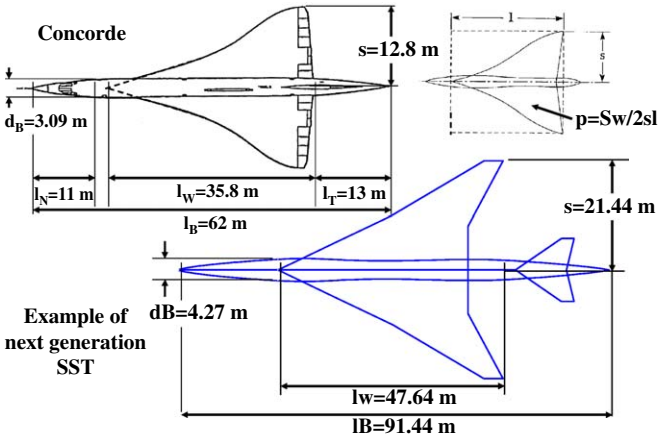

Fig. 2. Configuration parameters on Concorde and a next generation SST.

The formulation is summarized as follows [7]:

$$C_{Dwv} = \frac{512}{\pi}\left(\tau p \frac{s}{l}\right)^2 K_0\left(\beta\frac{s}{l}\right)\frac{S_{wet,each}/2}{S_w} \quad \text{for wing, tails} \tag{6}$$

where

$\frac{s}{l}$: semispan-to-length ratio (slendeness ratio)

$p \equiv \frac{Wing\ Area}{2sl}$: planform parameter

$\tau \equiv \frac{Volume}{(WingArea)^{3/2}}$: Volume parameter

$\beta \equiv \sqrt{M^2-1}$

K_0 : empirical coefficient for wave drag due to volume

Here, the parameters s/l and p that characterize the wing planform as shown in Fig. 2 are important to lift-dependent drag at supersonic speed, and τ is an essential parameter in wave drag due to volume if the empirical coefficient K_0 is nearly constant.

In the practical application of this formula, the coefficient K_0 is estimated using the following relation [6]. Comparisons with wind tunnel test data [7] have shown that this relation yields a good approximation.

$$K_0(x) \equiv 0.5114 - 0.4426\log_{10}x \quad 0.12 < x \le 1.0 \tag{7}$$

(ii) Body type

The wave drag due to volume for an axisymmetric body is estimated using the following relation [6]:

$$C_{Dwv} = \frac{4.69}{4}\left\{\left(\frac{d_{\max}}{l_N}\right)^2 + \left(\frac{d_{\max}}{l_T}\right)^2\right\}\frac{S_{cross}}{S_w} \quad \text{for fuselage} \tag{8}$$

where

$S_{cross} = \frac{\pi}{4}d_{\max}^2$, $d_{\max}$: maximum diameter

l_N *and* l_T : length of nose and tail parts

This was derived by referring to the statistical aerodynamic database called "DATCOM", which was developed in the United States and is used in many practical engineering fields.

2.1.2.3. Lift-dependent drag. According to lifting wing theory, lift-dependent drag is generally proportional to the square of lift coefficient for attached flow conditions. It is given by the following relation [7]:

$$C_{Dl} \equiv C_{Dwl} + C_{Dv} \equiv KC_L^2 \tag{9}$$

where

$$K \equiv \frac{1}{2\pi}\frac{p}{s/l}\left[2\beta^2\left(\frac{s}{l}\right)^2 K_W + K_V\right] \equiv \frac{K_L}{\pi AR}$$

$$\begin{cases} K_L \equiv \left[2\beta^2\left(\frac{s}{l}\right)^2 K_W + K_V\right] : \text{lift-dependent drag coefficient} \\ AR \equiv \frac{(2s)^2}{S_w} = \frac{2}{p}\left(\frac{s}{l}\right) : \text{aspect ratio} \end{cases} \tag{10}$$

The empirical coefficients K_V and K_W are well approximated by the following relations, which have been confirmed by wind tunnel test data [7].

$$K_W = \left(1 + \frac{1}{p}\right)\frac{f_w(\beta(s/l))}{2\beta^2(s/l)^2} \tag{11a}$$

$$f_w(x) = \begin{cases} 0.0, & x \le 0.178 \\ 0.4935 - 0.2382x + 1.6306x^2 - 0.86x^3 \\ \quad +0.2232x^4 - 0.0365x^5 - 0.5, & 0.178 < x \end{cases} \tag{11b}$$

$$K_V = \frac{1}{2}\left(1 + \frac{1}{p}\right) \tag{11c}$$

In addition, the following Küchemann's relation is also useful as a first approximation if Eq. (11) is not applied.

$$K_L = 0.75 + 2.55\frac{1}{2p}\left(\beta\frac{s}{l}\right) \tag{12}$$

2.1.3. Preliminary drag estimation

2.1.3.1. Drag characteristics of the Concorde. Before embarking on a preliminary study of the drag characteristics of a next generation SST, the effectiveness of the above drag formulations was firstly verified using the drag values of the Concorde. The configuration parameters of Concorde shown in Fig. 2 and Table 1 were estimated both by referring to technical information [8] and with some assumptions of JAXA. If the additional drag due to the propulsion system and airframe–propulsion interference is assumed to be about 0.002, the drag value estimated using the above formulations shows good agreement with the results in Ref. [9], as shown in Fig. 3. The additional drag was estimated by assuming the lift-to-drag ratio and cruise lift coefficient of Concorde are about 7 and 0.0125 at flight [8]. Here, the cruise lift coefficient was defined using exposed wing area as the reference area.

2.1.3.2. Drag characteristics of a next generation SST. In the preliminary drag study, several configuration parameters of a next generation SST were assumed referring to earlier studies by JADC and JAXA. In particular, JADC studied several design parameters taking into account aerodynamic and structural characteristics and flight and propulsion performance [5]. Table 1 shows representative requirements and some dimensions for a next generation SST compared with those of Concorde. The parameters used for drag estimation are summarized in the table as representative values of a reference configuration.

The estimated drag characteristics and lift-to-drag ratio are summarized in Figs. 4 and 5. Fig. 4 shows the effect on drag of varying the slenderness ratio, including the representative values. As shown in Fig. 4, there is an optimum slenderness ratio as described in Ref. [7], and its value is about 0.3 in this case. The existence of an optimum slenderness ratio is easily understood from Eqs. (9) and (10), because the wave drag due to lift

Table 1
Configuration parameters on Concorde and a next generation SST.

	Parameters	Concorde	Next Gen. SST
Flight conditions	M	2	2
	H (km)	15	15
	Reu (million:1/m)	8.07	8.07
	C_L	0.1($S_{ref} = S_W$), 0.125($S_{ref} = S_{exposed}$)	0.1($S_{ref} = S_W$)
Wing	S_W (m^2)	412.23	836.07 (9000 ft^2)
	$S_{exposed}$ (m^2)	329.78	
	s (m)	12.8	21.44
	AR	1.59	2.2
	s/lw	0.3575	0.35–0.45
	Pw	0.4497	0.318–0.409
	(t/c)av.	0.025	0.03
	τ	0.01322	0.0135
	M.A.C. (m)	21.59	25.04
	S_{wet} (m^2)	603.46	1672.14
	Re_{MAC} (million)	174.16	201.96
Fuselage	lB (m)	62	91.44 (300 ft)
	dB (m)	3.086	4.27
	lN/dB	3.56	4.5
	lT/dB	4.21	6
	S_{wet} (m^2)	523.6	1025.53
	Re_{lB} (million)	500.15	737.61
V-tail	Sv (m^2)	37.919	92.893
	sv (m)	5.39	8.77
	lv (m)	14.07	17.65
	sv/lv	0.3831	0.497
	Pv	0.25	0.3
	(t/c)av.	0.03	0.03
	τ	0.01142	0.0095
	M.A.C.(m)	9.38	10.6
	S_{wet} (m^2)	75.84	185.79
	Re_{MAC} (million)	75.67	85.44
H-tail	sh (m^2)	–	100.33
	sh (m)	–	6.8
	lh (m)	–	12.1
	sh/lh	–	0.562
	Ph	–	0.61
	(t/c)av.	–	0.03
	τ	–	0.0126
	M.A.C.(m)	–	7.38
	S_{wet} (m^2)	–	200.66
	Re_{MAC} (million)	–	59.55

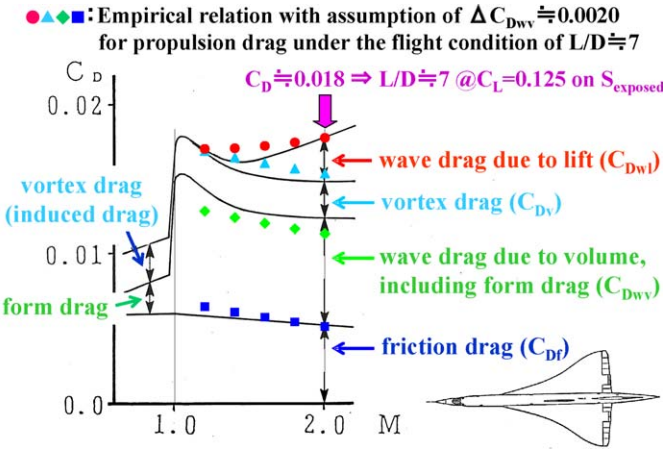

Fig. 3. Comparison of drag characteristics of Concorde [9] with estimated result by present empirical relation.

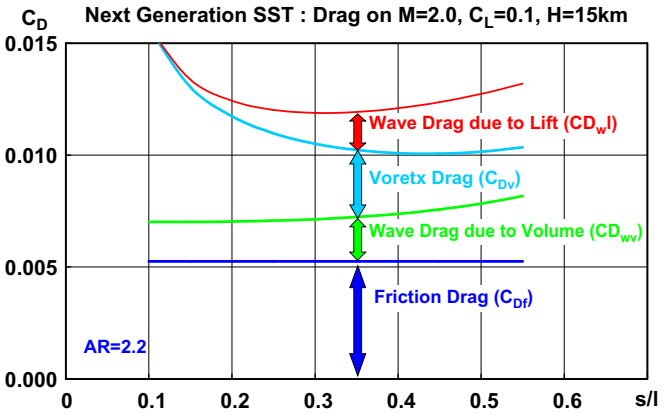

Fig. 4. Drag characteristics on slenderness ratio effect.

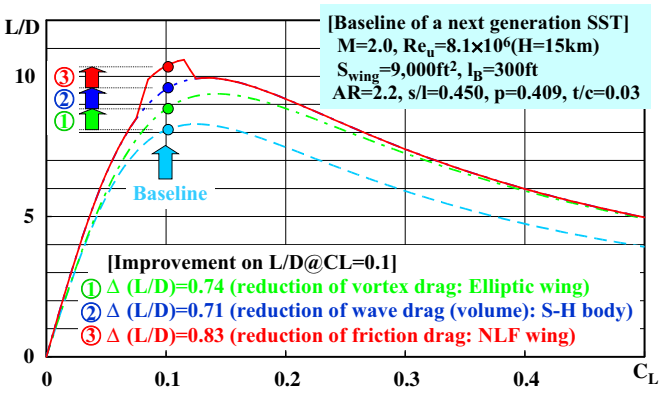

Fig. 5. Target of drag reduction effect on L/D characteristics of a next generation SST.

component is proportional to s/l while the vortex drag component is inversely proportion to s/l under the condition of constant empirical coefficients. On the other hand, there is no optimum aspect ratio, and a higher aspect ratio improves the lift-to-drag ratio as also estimated from those equations.

However, combining an optimum slenderness ratio with a higher aspect ratio is not easily realizable in a practical SST because of severe structural constraints. According to the JADC studies [4,5], slenderness ratios from 0.4 to 0.45 and aspect ratios from 2.0 to 2.5 are reasonable for a practical SST. Table 1 shows these values.

2.1.3.3. Maximum effect of drag reduction. Following the preliminary drag study, the maximum achievable drag reduction and the target lift-to-drag ratio were estimated by considering the reductions achievable for each drag component. The vortex drag reduction factor was selected to be 0.58. This is the theoretical optimum value achieved by using an elliptical planform to give minimum vortex drag according to Jones' wing theory [10]. Although a practical wing will have a slightly lower potential to achieve minimum vortex drag, vortex drag reduction is set as an aggressive target.

The reduction factor of wave drag due to volume was selected to be 0.64. This value assumes that the fuselage has the minimum wave drag due to volume characteristic of a Sears–Haack body, which was derived under the condition of the same volume and length as them of the fuselage [11]. However, additional interference wave drag will certainly be generated, and so the actual drag reduction factor achievable will be larger than 0.64.

The friction drag reduction factor is selected to be 0.84, corresponding to 60% laminar flow over the upper surface of the wing at the design condition, where the lift coefficient C_L is 0.1. In addition, the effective range of C_L was assumed to be from 0.08 to 0.12. The effect on drag of the proportion of laminar flow on the wing upper surface was estimated using the laminar friction coefficient on a flat plate.

The effects of these drag reduction measures are summarized in Fig. 5. The greatest L/D is about 10.6 at the design $C_L = 0.1$. This is a challenging target for JAXA's drag reduction research; in particular, greater laminar flow over the wing is one of the most effective means of improving L/D, but the concept of laminar flow over a wing with a subsonic leading edge at supersonic speed is a new one. This is therefore expected to be one of the most difficult, but at the same time one of the most rewarding, challenges. In the following sections, the reduction concepts for each drag component in JAXA's supersonic research activity are described in detail.

2.2. Drag reduction concepts

Since the development of the Concorde, much research has been carried out into reducing the pressure drag of supersonic aircraft. This has been mainly based on supersonic linear theory because the condition satisfied with linear approximation seems probably to give minimum drag. The following design concepts to reduce pressure drag according to supersonic linear theory are well known:

(1) The first concept is to select a slender, thin wing planform with a subsonic leading edge, which lies within the Mach cone generated at the apex of the wing. This requires a "planform study".
(2) The second concept is to design an optimum combination of camber and twist distributions over the wing. Such a curved wing is called a "warped wing". This requires a "warp study".
(3) The third concept is to design the fuselage cross-sectional area distribution to minimize drag increase due to wing–body interference. Such a fuselage with an adjusted area distribution is called an "area-ruled body". This requires an "area-rule study".

In general, the "planform" and "warp" studies are aimed at reducing lift-dependent drag and the "area-rule" study is aimed at reducing zero-lift pressure drag, that is, wave drag due to volume. Furthermore, the combination of these studies should be aerodynamically optimized to maximize the drag reduction effect.

Friction drag reduction is strongly required to improve the lift-to-drag ratio of an SST, but is difficult because boundary layer transition due to crossflow instability [12] near the leading edge of the highly swept SST wing is unavoidable, and so this is a challenging issue. An original design concept for a natural laminar flow (NLF) wing with subsonic leading edge was therefore developed in the NEXST program.

Each of the above-design concepts is now summarized below.

2.2.1. Arrow planform concept

In lifting surface theory [11], induced angle of attack and lift-dependent drag are generally formulated as follows:

$$\alpha_i(S) = \iint_{A_F} dS_1 K(S - S_1) l(S_1) : \text{induced AOA in forward flow} \quad (13)$$

where

$S \equiv (x, y)$: streamwise and spanwise coordinates

$dS \equiv dy\,dx$

$l(S) \equiv \Delta C_p(x, y)$: load

$$K(S - S_1) \equiv -\frac{1}{4\pi} \frac{x - x_1}{(y - y_1)^2 \sqrt{(x - x_1)^2 - \beta^2 (y - y_1)^2}}$$

$A_F(S_1)$: forward Mach cone region, $x_1 < x - \beta|y - y_1|$

$$C_{Di} = \frac{1}{S} \iint_{\sigma} dS\, l(S) \alpha_i(S) = \frac{1}{S} \int \int_{\sigma} dS\, l(S) \alpha_{iR}(S) \quad (14)$$

where

$$\alpha_{iR}(S) = \iint_{A_R} dS_1\, K(S_1 - S) l(S_1)$$

$K(S_1 - S) = -K(S - S_1)$

$A_R(S_1)$: rearward Mach cone region, $x_1 > x + \beta|y_1 - y|$

The above formulation for lift-dependent drag includes the well-known "reverse flow theorem", and α_{iR} indicates the local induced angle of attack in reverse flow [11].

Using the above equations and applying the variational principle to minimize C_{Di} at a given C_L, R.T. Jones derived the well-known minimum drag criterion [11];

$$\alpha_i(S) + \alpha_{iR}(S) = \text{const. for } S \quad (15)$$

This leads to the simple conclusion that the combined downwash induced in both forward and reverse flows is uniform over the entire wing. At subsonic speed, the minimum induced drag criterion is constant downwash, and the above equation means that the minimum induced drag criterion is the same for combined flow conditions in supersonic flow.

In 1952, Jones also derived that this criterion is achieved by an oblique elliptic planform [10]. As this was derived using supersonic linear theory, some corrections are needed when designing a practical wing. With a typical wing–body configuration, the oblique wing requires a variable sweep mechanism, but this increases structural weight and so this planform is generally not selected for practical wing designs. But present oblique elliptic planform concept is treated as the most challenging theoretical goal.

Excluding the oblique wing from the planform study, a higher aspect ratio is aerodynamically desirable at supersonic speed, which is easily derived by using the above Eqs. (9)–(11). Furthermore, an optimum s/l also reduces lift-dependent drag. Therefore, the first principle for reducing supersonic drag is to select a planform with optimum s/l and a relatively high aspect ratio. However, planforms with such an optimum slenderness ratio usually have highly swept leading edges, and this combined with a higher aspect ratio generally leads to some structural penalties.

Compromises in aspect ratio increase and slenderness ratio optimization are therefore necessary to build a practical wing within structural limitations. This implies that a relaxed guideline of selecting subsonic leading edge is only essential to reduce the drag and sensitivity of the s/l on the drag near the optimum value of s/l is very low. The arrow planform, with a subsonic leading edge at the inboard portions of the wing, is well recognised as an effective compromise. The arrow planform is similar to a delta planform with a small outer wing added to increase aspect ratio. Therefore, the modified first principle for reducing supersonic drag is to select an arrow planform with a suitable s/l near the optimum taking structural constraints into account.

One of the best ways to find a practical optimum planform is to design a number of candidates under prescribed constraints of aspect ratio, taper ratio, leading edge sweep angle and trailing edge sweep angle etc., and to compare their lift-dependent drag characteristics using a supersonic lifting surface method.

2.2.2. Warped wing concept

After a planform is chosen to reduce lift-dependent drag, the next approach to further reduce lift-dependent drag is to adopt a combination of wing camber and twist determined by an optimum wing load distribution. Such a cambered and twisted surface is often called "warped".

A number of analytical investigations performed about a half century ago obtained optimum load distributions on typical planforms such as delta, ogee and gothic types, for a number of aerodynamic constraints such as lowest drag, fixed aerodynamic centre and fixing trailing edge position [13,14]. However, these analytical solutions are not convenient for an arbitrary arrow planform. In 1964, Carlson et al. [15] developed a new numerical method for estimating drag and designing a warped surface, and improved it in 1974 [16]. This method is very effective for analyzing various planform and warp effects.

In Carlson's method, the load distribution over the wing is first approximated by summing several elementary load functions as follows:

$$\Delta C_p(x,y) \equiv l(S) = \sum_{n=1}^{N} c_n l_n(S) \tag{16}$$

where $l_n(S)$: nth elementary load function

Applying the variational method with the Lagrange multiplier technique to minimize lift-dependent drag at a given lift, each combination of coefficients is estimated by the following equation:

$$c_n = k \sum_{m=1}^{N} A_{nm}^{-1} C_{L,m} \tag{17}$$

where

k : Lagrange multiplier

$$C_{L,m} \equiv \frac{1}{S} \int \int_{\sigma} dS\, l_m(S) \tag{18}$$

$$A_{nm} \equiv C_{Di,nm} + C_{Di,mn} \tag{19}$$

$$C_{Di,nm} \equiv \frac{1}{S} \iint_{\sigma} dS\, l_n(S) \alpha_{i,m}(S) = \frac{1}{S} \int \int_{\sigma} dS\, l_m(S) \alpha_{iR,n}(S) \tag{20}$$

$$\begin{cases} \alpha_{i,m}(S) = \iint_{A_F} dS_1\, K(S - S_1) l_m(S_1) \\ \alpha_{iR,n}(S) = \iint_{A_R} dS_1\, K(S_1 - S) l_n(S_1) \end{cases}$$

The above procedure is mathematically the same as the derivation of Jones's minimum drag criterion [11] but with fewer elementary loads; e.g. $N = 8$ in Carlson's 1974 method versus $N = \infty$ with Jones's theoretical consideration. The drag of a warped surface designed by Carlson's method is therefore generally larger than the theoretical minimum given by Jones, and a preliminary numerical study by the author found that Carlson's method achieved about 85% of the theoretical maximum drag reduction, which is the difference between the drag of a flat plate and Jones's optimum value.

The key point of the warped design for reducing drag is the suppression of theoretically infinite load at the leading edge. Because a separation vortex is generally induced on a highly swept leading edge by a local high angle of attack, a certain amount of leading edge droop becomes necessary to achieve attached flow at the leading edge. This is the second principle for reducing supersonic drag.

Finally, the following general feature of the lift-dependent drag characteristics of a warped wing is derived using supersonic lifting surface theory. In linear theory, the influence of angle of attack α_f is reflected through the combination of the following two loads:

$$l(S) = l_w(S) + l_f(S) \tag{21}$$

$l_w(S)$: prescribed load at a warp design condition
$l_f(S) = l_{u,f}(S)\ \alpha_f$: load at a flat plate condition

This means that the dependence of α_f on load is the same as for a flat plate, naturally supposed in linear theory. Under this assumption, lift and lift-dependent drag coefficients are formulated as follows:

$$C_L = C_{Ldes} + C_{Lf} \tag{22}$$

where

$$C_{Ldes} = \frac{1}{S} \iint_{\sigma} dS l_w(S)$$

$$C_{Lf} = C_{L\alpha f} \alpha_f,\ \ C_{L\alpha f} = \frac{1}{S} \iint_{\sigma} dS l_{uf}(S)$$

$$C_{Di} = K(C_L - C_{L0})^2 + \Delta C_{Di} \tag{23}$$

where

$$K \equiv \frac{1}{C_{L\alpha_f}},\ \ C_{L0} \equiv \frac{C_{Ldes} - \lambda}{2},$$

$$\Delta C_{Di} \equiv C_{Di,des} - K\left(\frac{C_{Ldes} + \lambda}{2}\right)^2$$

$$\lambda \equiv \frac{1}{S} \iint_{\sigma} dS l_{uf}(S) \alpha_{i,des}(S), C_{Di,des} \equiv \frac{1}{S} \iint_{\sigma} dS l_w(S) \alpha_{i,des}(S)$$

$$\alpha_{i,des}(S) = \iint_{A_F} dS_1 K(S - S_1) l_w(S_1)$$

These formulations have some remarkable features.

(i) The lift slope $C_{L\alpha}$ equals that of a flat plate.
(ii) K, which characterizes a polar curve, is the inverse of the lift slope and is also the same as for a flat plate.
(iii) The drag reduction effect at a design value of C_L increases as C_{L0} increases, unless ΔC_{Di} increases excessively.

2.2.3. Area-ruled body concept

In the above, a thin and slender wing and fuselage were chosen to reduce wave drag due to volume following linear theory indicating that certain aerodynamic configurations have lower drag. A third principle is now applied to further reduce wave drag, namely the so-called "area-rule" technique for fuselage design. This reduces the drag due to volume that arises from interference drag between the wing, tails and fuselage.

According to supersonic slender body theory [11], wave drag due to volume is generally expressed as the following:

$$D_W = -\frac{q}{4\pi^2} \int_0^{2\pi} d\theta \int \int_0^{l} S''(x_1,\theta) S''(x_2,\theta) \ln|x_1 - x_2| dx_1\, dx_2 \tag{24}$$

where

$S'' \equiv \dfrac{d^2S}{dx^2}$

q : dynamic pressure

Here θ is one of the coordinates that define the Mach cone (the other coordinates being the apex angle related to Mach angle and distance from the apex), and S is the projection of the oblique cross-sectional area cut by each Mach plane on a plane perpendicular to the streamwise direction. (For convenience, this is called "supersonic area".) This formulation was derived by von Karman and Hayes assuming a body with a pointed tail.

In general, a fuselage is approximately axisymmetric while the wing and tails are non-axisymmetric. Then, the following relations are assumed:

$$S(x,\theta) = S_f(x) + S_W(x,\theta) \tag{25}$$

where

S_f : supersonic area of fuselage

S_W : supersonic area of wing, $H-$tail, $V-$tail

and Fourier expansion : $S'_W(x,\theta) = \sum_{n=0}^{\infty} A_{2n}(x)\cos(2n\theta)$

$$A_{2n}(x) = \frac{1}{2\pi}\int_0^{2\pi} S'_W(x,\theta)\,\cos(2n\theta)\,d\theta$$

Under these assumptions, wave drag is expressed as follows:

$$D_W = D_{Wing-Body} + (D_{Wing})_n \tag{26}$$

where

$$D_{Wing-Body} \equiv -\frac{q}{2\pi}\int\int_0^l \left\{S''_f(x_1) + A'_0(x_1)\right\}\left\{S''_f(x_2) + A'_0(x_2)\right\} \times \ln|x_1 - x_2|\,dx_1\,dx_2$$

$$(D_{Wing})_n \equiv -\frac{q}{4\pi}\sum_{n=1}^{\infty}\int\int_0^l A'_{2n}(x_1)A'_{2n}(x_2)\ln|x_1 - x_2|\,dx_1\,dx_2$$

If wing and tails are specified, it is difficult to reduce the second term $(D_{wing})_n$ due to their non-axisymmetric characteristics. On the other hand, the first term $D_{wing-Body}$ corresponds to an axisymmetric component. For this term, a body with an optimum area distribution is called a "Sears–Haack body". Therefore, if the first drag term in Eq. (26) is that of a Sears–Haack body, the wave drag due to volume of the whole configuration will be reduced.

To achieve this, it is necessary to modify the fuselage geometry as described below:

$$S''_f(x) + A'_0(x) = S''_{SH}(x) \tag{27}$$

$$\therefore\ \{S_f(x)\}_{Area-Ruled} = S_{SH}(x) - S_0(x)$$

where

$$S_0(x) \equiv \int_0^x A_0(x')\,dx' = \frac{1}{2\pi}\int_0^{2\pi} S_W(x,\theta)\,d\theta$$

$$S_{SH}(x) \equiv \frac{128V_{tot}}{3\pi l}\left\{\frac{x}{l}\left(1-\frac{x}{l}\right)\right\}^{3/2} : \text{ Sears-Haack body}$$

where V_{tot} is total volume of the whole configuration. This improved fuselage is generally called an "area-ruled" body. This rule is the third principle for reducing supersonic drag.

2.2.4. Natural laminar flow (NLF) wing concept

It is expected that an aerodynamically optimum combination of the above pressure drag reduction concepts will greatly reduce supersonic cruise drag, but it is not easy to obtain the maximum theoretical drag reduction effect because a number of constraints that are not included in linear theory must be taking into account. Therefore, friction drag must also be reduced.

Laminar airfoil design is usually based on suppressing Tollmien–Schlichting (T–S) wave instability. For a low aspect ratio wing with highly swept leading edges, transition due to crossflow (C–F) instability is dominant over the forward part of the wing [12]. Therefore, an optimum pressure distribution to suppress the C–F instability must first be found. While it is generally impossible to eliminate crossflow entirely, the key aim is to reduce the size of the region that generates crossflow. Crossflow is produced by any chordwise pressure gradient. There is always severe acceleration over the forward part of the wing, and narrowing the region of acceleration will reduce crossflow. This leads to a pressure distribution with steep gradient at the front.

Since T–S instability becomes dominant after the mid-chord, gradual acceleration will be effective in suppressing it. Fortunately, most SST planforms have supersonic trailing edges and require no pressure recovery there.

At the first step of our NLF wing design, an optimum pressure distribution to delay transition was found [17] according to the above considerations using a transition analysis code (SALLY code [18]) based on the e^N method. The SALLY code predicts the so-called N-factor for both T–S instability and C–F instability. The N-curve means the envelope formed by integrating the rates of amplification of small disturbances over a wide range of frequencies. As transition is physically caused by such amplified disturbances, it is expected that there is a certain correspondence between the transition point (the exact onset of transition) and the N-factor. This N-factor is not predicted by any theory but is empirically estimated through flight tests or quiet wind tunnel tests. Although a body of information has been gathered relating to the N-factor for the two-dimensional subsonic speed regime, there is little data on three-dimensional flow at supersonic speed and so at present the location of the transition on this optimum pressure distribution cannot be predicted from the N characteristics. However, the lower N-factor estimated using SALLY code shows that the optimum pressure distribution described in Ref. [17] has better transition characteristics.

The SALLY code is formulated in incompressible theory, so a new compressible stability code was developed by JAXA for the NEXST program. The optimum pressure distribution was also investigated using this compressible stability code and its validity was confirmed.

As the next step, a so-called inverse design problem that achieves the optimum pressure distribution must be solved. In the NEXST program, an original CFD-based inverse method was developed [19–21]. This consists of iterating over the following two routines: (i) flow estimation using a CFD code, and (ii) modifying the wing geometry based on the differences between the target and each estimated pressure distribution using supersonic linear theory. The supersonic NLF wing design is the fourth principle for reducing supersonic drag.

2.2.5. Summary of drag reduction concepts

Taking account of the features of lift-dependent drag, the formulation of total drag at supersonic speed is summarized as follows:

$$C_D = K(C_L - C_{L0})^2 + C_{D\min} \tag{28}$$

Then, according to this expression, the following general condition for maximum lift-to-drag ratio is derived:

$$\left(\frac{L}{D}\right)_{\max} = \frac{C_{Lopt}}{C_{Dopt}} = \frac{1}{2K(C_{Lopt} - C_{L0})} = \frac{1}{2}\left(\sqrt{\left(\frac{C_{L0}}{C_{D\min}}\right)^2 + \frac{1}{KC_{D\min}}} + \frac{C_{L0}}{C_{D\min}}\right) \tag{29}$$

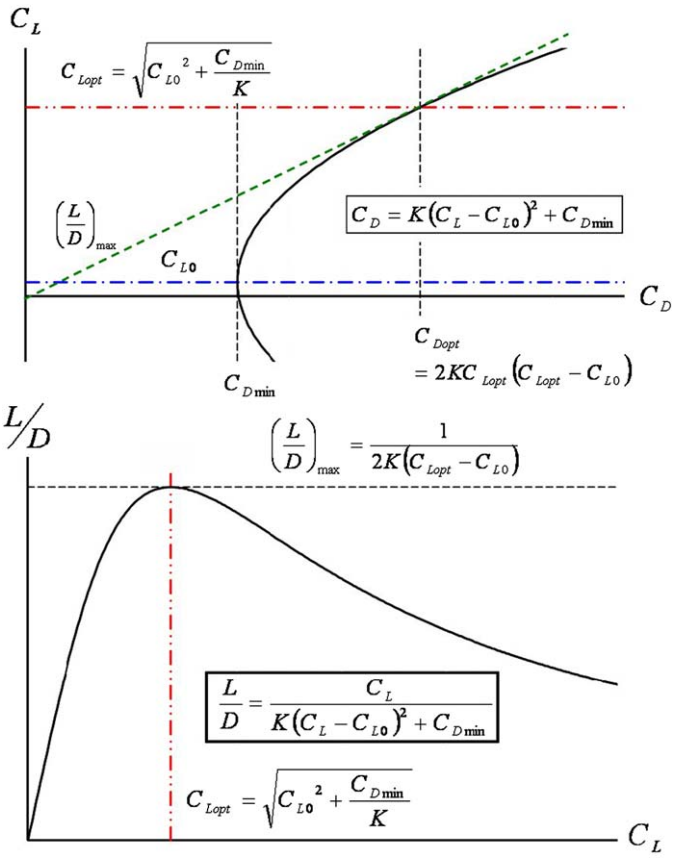

Fig. 6. General features of drag and L/D characteristics.

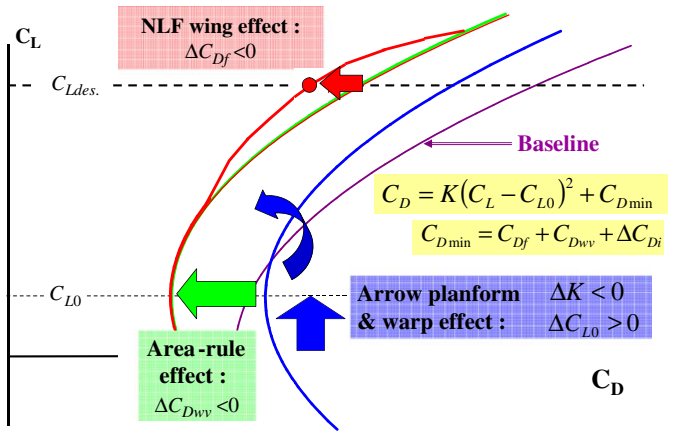

Fig. 7. Effect of each drag reduction concept.

where

$$C_{Lopt} = \sqrt{C_{L0}^2 + \frac{C_{Dmin}}{K}}$$

$$C_{Dopt} = 2KC_{Lopt}(C_{Lopt} - C_{L0})$$

The general features of these equations are shown schematically in Fig. 6. Eq. (29) indicates that increasing C_{L0} and decreasing both K and C_{Dmin} will increase the maximum L/D. If a thin wing approximation is assumed, K is exactly equal to the inverse of lift slope $C_{L\alpha}$ as shown in Eq. (23). (In the case of a thick wing, K is a function of both lift slope and thickness ratio as indicated in Ref. [22].) In general, a wing with a higher aspect ratio has a greater lift slope. Therefore, the condition for reducing K, namely increasing $C_{L\alpha}$, corresponds to increasing aspect ratio.

An increase of C_{L0} is achieved by designing strongly curved wing surfaces, but such a warped wing generates unavoidable additional vortex drag ΔC_{Di} according to Eq. (23). This drag is added to C_{Dmin}, and so a relatively greater C_{L0} does not always give a better solution. Finally, the effect of each drag reduction concept on each term of the drag formulation is summarized in Fig. 7.

3. Non-powered scaled supersonic experimental airplane project by JAXA

As mentioned above, the NEXST program began in 1997 and continued until 2006. Its main objectives were to develop an advanced CFD-based aerodynamic design technique for achieving high lift-to-drag ratio and to validate its effectiveness by flight tests. The structure of the program is shown in Fig. 1, and included fundamental research activities and two flight test projects using different scaled experimental airplanes [1,2]; the non-powered (NEXST-1) airplane and the jet-powered (NEXST-2) airplane.

The first flight of the NEXST-1 airplane on 14 July 2002 failed, and the NEXST-2 project was subsequently cancelled. After reconfirming and redesigning the whole NEXST-1 airplane system over about 3 years, the second flight on 10 October 2005 was successful. As a result, only the NEXST-1 design technique was flight validated, but the NEXST-2 design technique was at least partially validated by wind tunnel tests. This chapter presents the aerodynamic design and flight test results of the NEXST-1 airplane.

3.1. Aerodynamic design process and results

The main target for the aerodynamic design of the NEXST-1 airplane was to reduce supersonic drag. In the NEXST program, JAXA developed advanced aerodynamic design techniques according to the following philosophies: to design mathematically using a logical process without any empirical parameters, and to incorporate innovative techniques that exceed the technology of the Concorde. Firstly, a CFD-based design technique was developed including both pressure and friction drag reduction concepts as described in the previous chapter. Those design concepts led to an arrow planform, a warped wing, an area-ruled body and a natural laminar flow (NLF) wing. The application of an NLF wing concept to an SST configuration with a subsonic leading edge was the first application in the world [23].

Before designing the NEXST-1 airplane, some design requirements for a full-size SST first had to be specified. According to the study [5] by JADC, which was sponsored by the Society of Japanese Aerospace Companies (SJAC) and some overseas studies [24,25], the following dimensions were finally selected for a next generation SST.

- Cruise Mach number: $M = 2$
- Cruise lift coefficient: $C_L = 0.1$
- Flight altitude: $H = 15$ km
- Wing area: $S = 9000\,\text{ft}^2$
- Fuselage length: $L = 300$ ft
- Fuselage volume: $V = 30000\,\text{ft}^3$ (for 300 pax.)
- Tail configurations: scaled shapes of Concorde and some planned next generation SSTs.

JAXA then selected a scale ratio of 11% of the full-size SST dimensions above for the NEXST-1 airplane primarily considering budget constraints. However, the tail cone length of the scaled

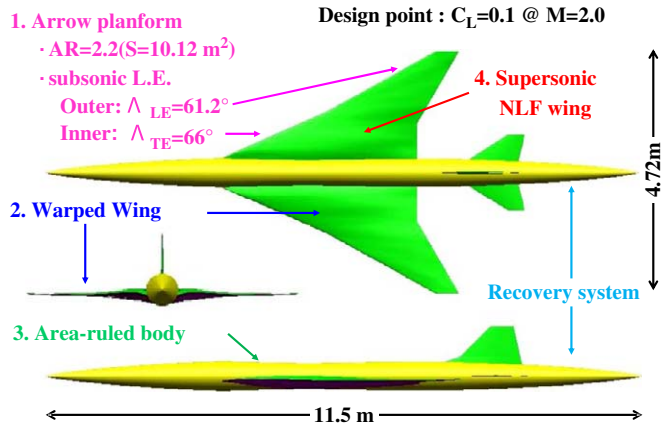

Fig. 8. Aerodynamic design concepts and configuration of NEXST-1 airplane.

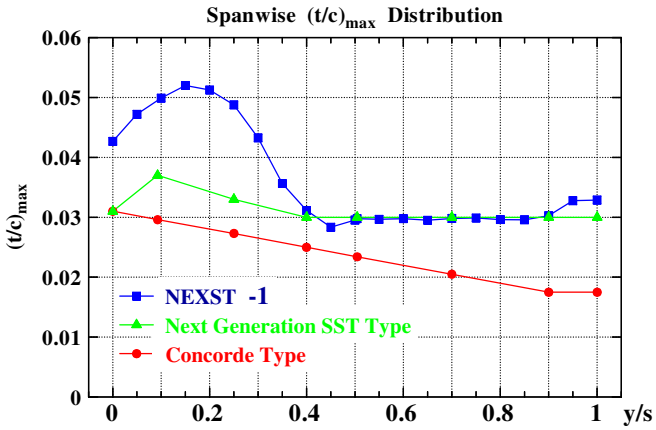

Fig. 10. Each spanwise distribution of maximum thickness ratio.

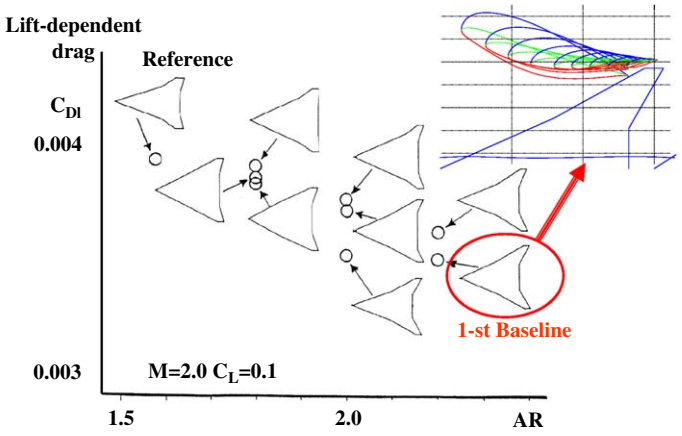

Fig. 9. Principal results on both planform and warp studies.

fuselage was extended slightly to allow the installation of a parachute system to recover the airplane after flight test. In addition, the fuselage diameter was increased to 110% of diameter of the scaled fuselage based on the above dimensions. Therefore, the tail shape of the scaled airplane differs to that of the full-size SST.

The aerodynamic design process of the NEXST-1 airplane consisted of two phases [23]. A baseline configuration was first designed incorporating three pressure drag reduction concepts using a supersonic linear theory and a CFD (Navier–Stokes (NS)) code. Then, JAXA improved the lift-to-drag ratio (L/D) by applying the NLF wing concept using an original CFD-based inverse design method. These design concepts and the final designed configuration are summarized in Fig. 8. The design results of each process are described in the following sections.

3.1.1. Pressure drag reduction design (baseline configuration design)

3.1.1.1. Planform design. In general, an arrow planform is characterised by the parameters wing area (S), aspect ratio (AR), slenderness ratio (s/l), taper ratio (λ), leading edge sweep angle (Λ_{LE}), trailing edge sweep angle (Λ_{TE}), and spanwise kink positions at both leading and trailing edges (ε_L, ε_T). In the planform study, some of these parameters were determined referring to a typical arrow planform (indicated as "Reference" in Fig. 9), AR, s/l, Λ_{LE},i (for the inner wing), Λ_{TE},o (for the outer wing) and ε_T (for the trailing edge) were selected as the major parameters. A value of $\Lambda_{TE} = 0^\circ$ was set for the inner wing due to structural constraints. For s/l, a near optimum value of about 0.3 at the chosen cruise Mach number (see Fig. 4) was initially selected, but considering structural constraints an s/l range from 0.3 to 0.5 was investigated. Furthermore, AR values from 1.8 to 2.2 were considered to achieve a moderate balance between aerodynamics and structure.

Ninety-nine planform candidates were generated geometrically according to these considerations and their lift-dependent drag characteristics were estimated and evaluated as a flat plate using lifting surface theory [16]. One criterion for selecting an optimum planform was to pick those planforms with better low-drag characteristics than the reference planform. Another criterion was to select planforms having low sensitivity of its drag to Mach number at the design point. Through this analysis, eight planforms apart from the "Reference" planform were selected for the next design step, as summarized in Fig. 9.

3.1.1.2. Warp design. For each of the eight planforms derived from the planform study, a warped surface was designed and its lift-dependent drag was estimated at the design point using Carlson's method [16]. As mentioned in the previous chapter, Carlson's method gives an optimum load distribution for a given planform. The local induced angle of attack distribution was easily estimated by supersonic lifting surface theory, and used to derive a warped surface composed of camber and twist distributions. The planform with the lowest drag was finally selected with $AR = 2.2$ and $\Lambda_{LE} = 66/61.2$ degrees (inner/outer wing), and is indicated as "1st Baseline" in Fig. 9.

In order to design a complete warped wing, chordwise and spanwise thickness distributions are necessary. The spanwise thickness ratio distribution was determined by referring to the thickness ratio distributions of another country's planned next generation SST configurations [24,25] rather than that of Concorde. This has a thickness ratio of 3.7% near the wing root to allow space for landing gear and 3% at the outer wing to satisfy structural constraints. The spanwise thickness ratio distributions of this next generation SST and Concorde are shown in Fig. 10 [23]. For the chordwise thickness distribution, JAXA applied that of the NACA 4-digit series because it has a simple analytical expression. Fig. 9 also schematically indicates the airfoil shape of the designed warped wing at each spanwise station.

3.1.1.3. Area-ruled body design. Before the area-ruled body design, the locations of the horizontal/vertical tail and wing were

determined by reference to similar overseas planned SST configurations. As an initial fuselage configuration, a straight cylindrical fuselage except for the nose and tail cones that met the fuselage volume requirement was assumed. Then, a supersonic cross-sectional area distribution of the area-ruled body was estimated according to the design procedure mentioned above. Fig. 13 shows all components of the supersonic area distributions. The area of a Sears–Haack body of the same volume as the initial fuselage with wing and tails was estimated. The area distribution of the area-ruled body was then calculated by subtracting the area of the wing and tails from the area of Sears–Haack body. Finally the area-ruled body configuration was determined from the estimated area distribution with an axisymmetrical body approximation. This wing–body–tails configuration was called "1st Configuration" [23].

3.1.1.4. Refinement using CFD analysis. Since the 1st Configuration was designed with concepts based on supersonic linear theory, the drag reduction effect of these concepts was verified with a JAXA-developed CFD (Navier–Stokes) code [26] under the fully turbulent condition. The following major differences between the drag reduction predicted by linear theory and CFD were found [27]: (i) loss of total lift at a given angle of attack, (ii) increase in minimum drag, and (iii) loss of lift at the minimum drag condition. The differences mainly originated due to the influences of wing thickness and the body, particularly the strong interference of an area-ruled body with static pressure on upper surface, because these effects are not included in linear theory. The (ii) and (iii) above mean reduced effectiveness of the wing warp. The main reason is a load deficit near the leading edge compared with the optimum load designed by Carlson's method.

To improve the drag characteristics of the 1st Configuration, the camber was modified to remove the load deficit near the leading edge. A simple quasi-inverse method formulated by two-dimensional supersonic linear theory was used for this purpose, and applied to the wing section at each 5% semispan location [27,28]. The target load distribution was recalculated to treat the effect of the fuselage on warped surface using Middleton and Lundry's method [29], which is an extension of Carlson's method that includes wing–fuselage interference. Furthermore, the chordwise thickness distribution was replaced with the distribution of a NACA 66-series airfoil, which is one of laminar airfoils at low speed, because it was found to have better transition characteristics in supersonic flows [27]. This redesigned configuration was called "2nd Configuration", and is an aerodynamically optimum configuration designed with present pressure drag reduction concepts [23,27].

3.1.2. Friction drag reduction design (CFD-based inverse design)

3.1.2.1. Application of natural laminar flow (NLF) wing design. In order to reduce the drag of the 2nd Configuration still further, JAXA developed an original complete three-dimensional inverse design method to achieve the optimum pressure distribution derived in the preliminary design study [17]. This inverse method uses CFD analysis to compute the flow field around the complete configuration (wing–body–tails) and a geometry modification procedure applied to the wing alone [19–21]. The governing equation of the modification procedure is based on supersonic lifting surface theory and solved using a panel method. Although this design method is applied only to the wing design, it maintains the pressure drag reduction effect incorporated in the design of the baseline configuration by carrying out CFD analysis of the complete configuration at each iteration. Therefore, the final designed configuration is expected to include both pressure and friction drag reduction effects.

Fig. 11 shows the design flow of the CFD-based inverse design procedure and its results. The target pressure distribution on the wing upper surface was the optimum pressure distribution for the NLF wing, and the target pressure distribution on the lower surface was obtained by subtracting the optimum load distribution estimated by Middleton and Lundry's method from the upper surface target pressure distribution. The 2nd configuration was used as the initial configuration [23].

Each iteration loop consists of the following steps: (1) The pressure distribution on the wing surface of the configuration is estimated using a JAXA CFD solver with turbulent flow conditions; (2) the pressure difference between the estimated and optimum pressure distributions is calculated; (3) the required geometry correction is derived from the pressure difference using the inverse method; (4) the wing section geometries at 14 spanwise stations are modified by adding the correction to the configuration; and (5) a new configuration incorporating the modified wing

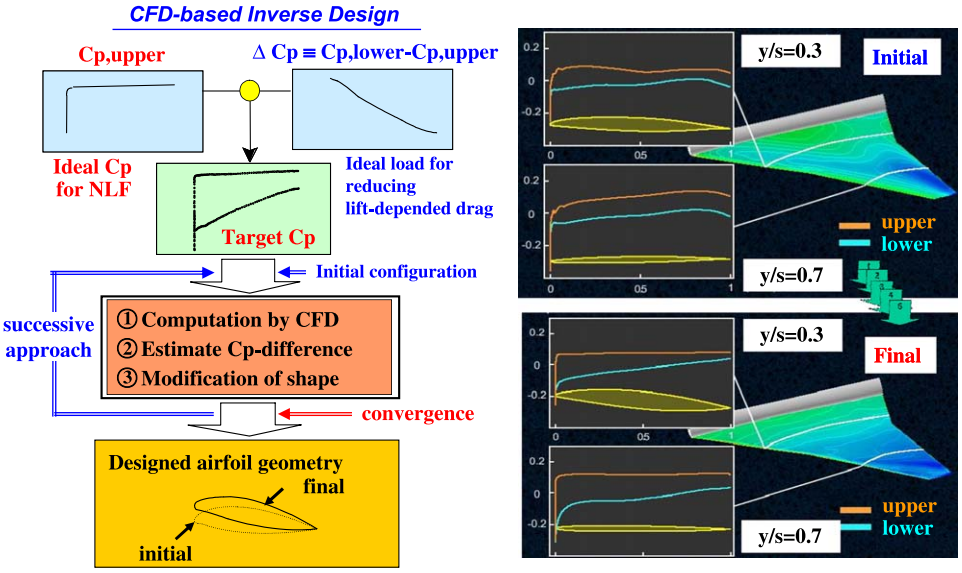

Fig. 11. Design flow of CFD-based inverse design method.

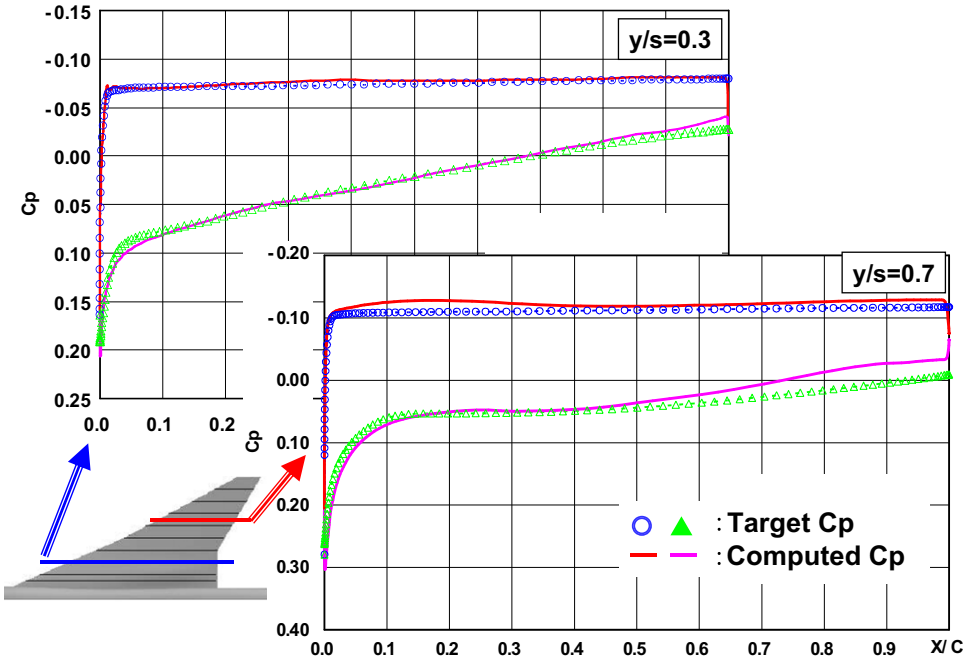

Fig. 12. Final results of Cp distributions by present inverse design.

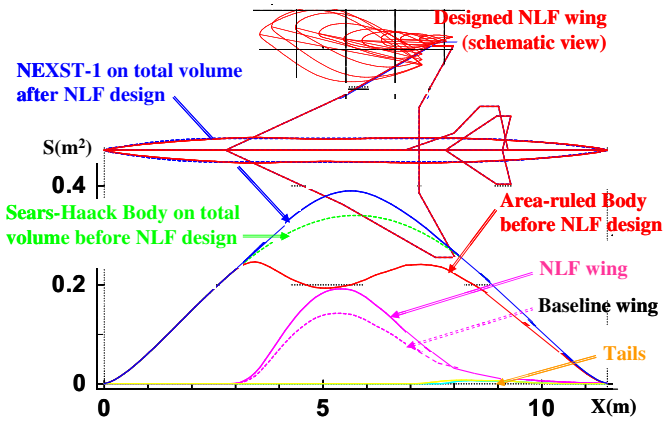

Fig. 13. Final configuration designed by present inverse method.

geometry and the original fuselage is defined by a smoothing process using the "CATIA" three-dimensional geometry generation software. Most of the time is spent in step (5), and a single iteration including CFD analysis required about 1 week.

When this procedure was first applied, the inboard wing became thicker while the outboard wing became thinner at each iteration loop. These modifications did not conform to the prescribed spanwise thickness ratio distribution, and meant that present NLF wing design method was mathematically ill-posed; to be precise, the target pressure distribution could not be satisfied by a wing shape constrained by both the warp condition and the prescribed spanwise thickness ratio distribution. Solving this problem requires the target pressure distribution to be modified, but it was not easy to find another pressure distribution that delayed transition while satisfying the wing shape constraints. Instead, as an approximation, the maximum thickness of the modified wing geometry was adjusted to the prescribed maximum thickness during the CATIA smoothing process.

The wing configuration after ten iterations was selected as the final configuration. Fig. 12 compares the pressure distribution of this final configuration with the target, and it was judged that the iterative process had achieved good convergence. The wing section geometry and area distributions of the final configuration are shown in Fig. 13 and its spanwise thickness ratio distribution is also shown in Fig. 10. The designed thicker thickness ratio distribution at inboard wing region was not adjusted to the prescribed thickness ratio distribution. This resulted in a considerable deviation from the ideal Sears–Haack body supersonic area distribution as shown in Fig. 13, and consequently in an increased wave drag due to volume. However, JAXA recognised that the validation of the original NLF wing design concept was more valuable than the validation of classical area-ruled body design concept in flight test [23].

3.1.2.2. Transition analysis. In order to evaluate the transition characteristics of the final configuration, because the SALLY code used in finding the optimum Cp distribution for the NLF wing is formulated in incompressible stability theory, JAXA developed a new compressible e^N code called the LSTAB code [30]. Fig. 14 shows the transition characteristics of the final configuration predicted by LSTAB with $N = 14$ as the criterion for determining transition locations. This criterion was chosen referring to NASA's Low Disturbance Supersonic Tunnel test results [31]. In this prediction, a maximum limit of 60% chord was specified for the delayed transition point due to some practical constraints. The figure shows a larger laminar region on the wing upper surface at the design angle of attack (2°) and at 3° in the flight test conditions.

Since this was the first time transition measurement in supersonic flight had been attempted in Japan, an effective and reliable transition measurement system was carefully designed to clearly detect the transition characteristics. Four types of transition detection sensor were selected to compare their performance: hot-film (HF), dynamic pressure transducer (DP), thermocouple (TC), and Preston tube. The sensor locations, shown in

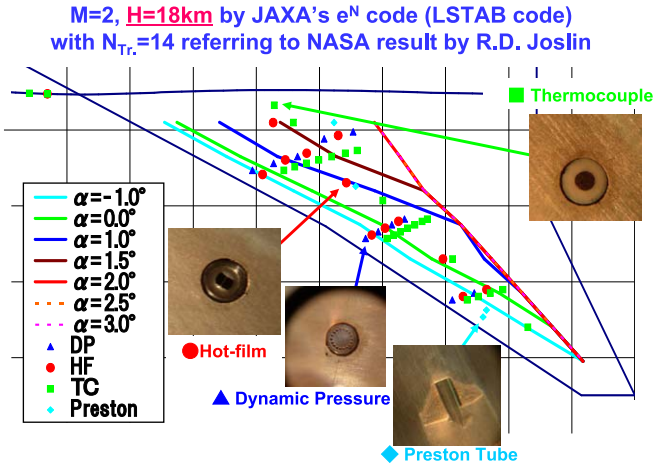

Fig. 14. Transition prediction results at flight test condition.

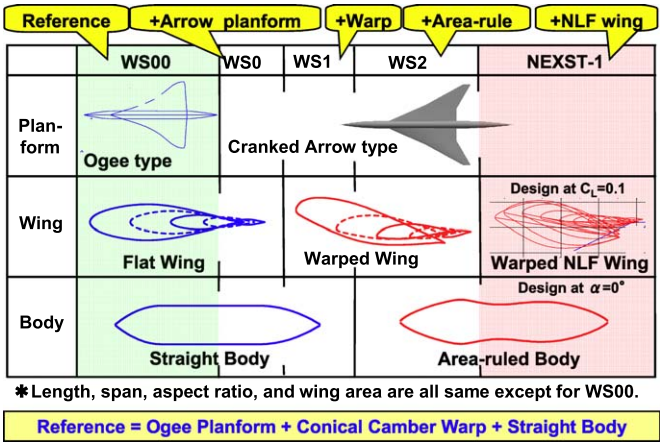

Fig. 15. Each configuration based on each drag reduction concept.

Fig. 14, were determined from the predicted transition locations under flight test conditions.

The possibility of transition due to attachment-line contamination in the flight test was also considered. This generally originates in the turbulent boundary layer on the fuselage surface, and although it is not predicted precisely by any theories, Poll's method [32] based on some empirical relations is known to be practical. Using Poll's criterion, transition due to attachment-line contamination on the wing of the final configuration was predicted in a small spanwise region of the inner wing at the flight test condition of $H = 15$ km, but not at higher altitudes [33]. The validity of these predictions was expected to be verified in the flight test.

3.1.3. Summary of drag reduction effects

In order to precisely understand the quantitative drag reduction effects of the JAXA aerodynamic design technique, the drag characteristics of each configuration due to each concept were again analyzed using JAXA's CFD code. Figs. 15 and 16 show each designed configuration and its corresponding drag characteristics. By comparing with a reference configuration designed with a flat Ogee planform and a non-area-ruled body, the effect of each drag reduction concept was estimated as follows: an approximately 11.5 counts reduction due to the Carlson's warped arrow wing, an approximately 6.7 counts reduction due to the area-ruled body,

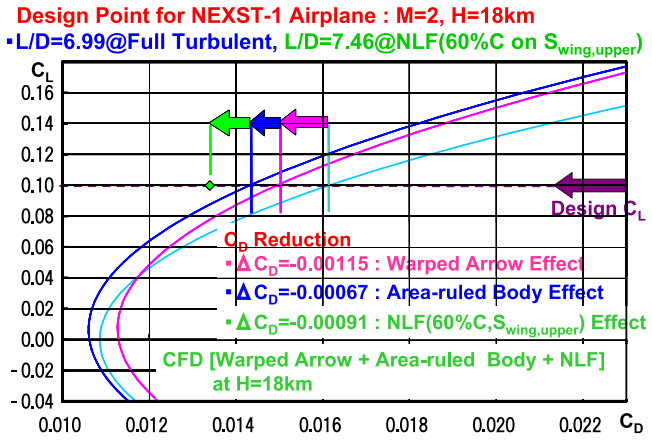

Fig. 16. Each drag reduction effect on each configuration.

and an approximately 9.1 counts reduction due to the effect of the NLF wing assuming 60% laminar flow over the upper surface.

3.1.4. Validation of concepts in wind tunnel tests

Several wind tunnel tests were conducted to complete the aerodynamic design of the NEXST-1 vehicle. The detailed results are summarized in reference [34,35]. In this section, the principal results confirming the NLF wing design concept are summarized.

It is not easy to conduct transition measurement tests in a typical blow down supersonic wind tunnel due to a certain level of freestream turbulence. However, it was thought that a continuous flow tunnel would give sufficiently low freestream turbulence and so the transition measurement test was conducted at ONERA's "S2MA" supersonic closed-circuit tunnel. As this had the largest test section among the several tunnels available to JAXA, a relatively large wing–body configuration model at 23.3% scale of the NEXST-1 airplane was constructed as shown in Fig. 17.

The pressure distribution at the design condition was first investigated. Fig. 17 compares CFD analysis results with the wind tunnel measured Cp distributions of two models; an 8.5%-scale complete configuration model at JAXA's supersonic wind tunnel and the 23.3%-scale wing–body model at ONERA-S2MA. As the figure shows, there is very good agreement between these and it is confirmed that the designed configuration realised the target Cp distribution.

Transition characteristics were then investigated in the S2MA. The infra-red (IR) image technique as well as multi-element hot-film sensors were used to detect the transition location. The total pressure fluctuation measured by a dynamic pressure transducer placed on the model was about 0.29%. Even though this value is not so small, we clearly confirmed the rearward movement of the transition location at the design point condition (AOA $= 2.0^\circ$) as shown in Fig. 18 [35]. Naturally, it was understood that the amount of the transition movement was not the same as the LSTAB prediction because of the freestream turbulence.

3.1.5. Manufactured configuration design

In the aerodynamic design of the flight test airplane, consideration was given to the effect of aeroelastic deformation. In the aeroelastic design procedure for the full-scale NEXST-1 airplane, NSTRAN was used to estimate elastic deformation due to inertial and aerodynamic loads at the design point $H = 18$ km, the altitude at which the first aerodynamic measurements were planned to be carried out.

For analysis, a "Jig Shape" (referred to as "JS" below) to be used for manufacturing the NEXST-1 airplane was first defined by subtracting the aeroelastic deformation from the designed

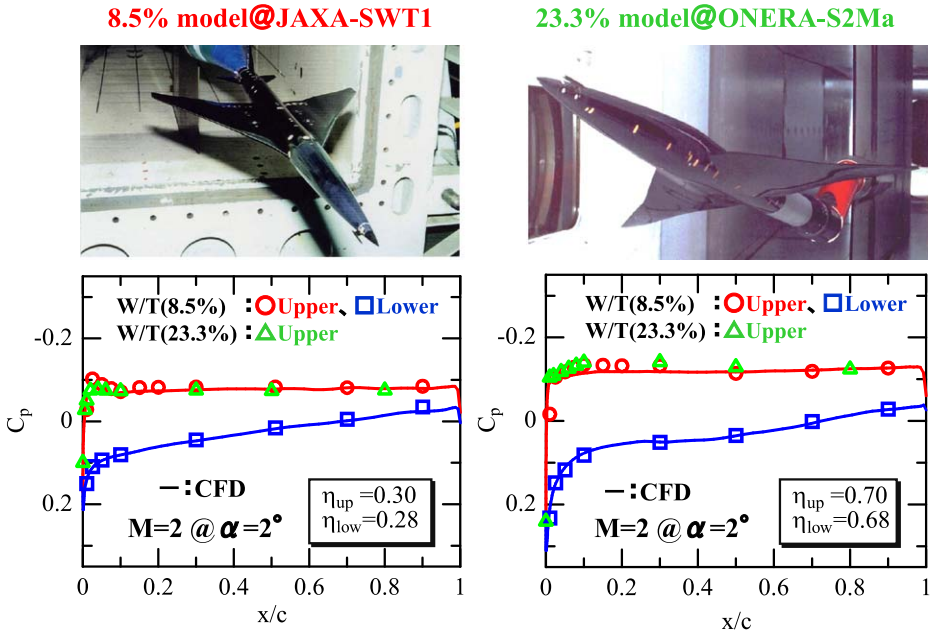

Fig. 17. Experimental validation test for pressure distribution.

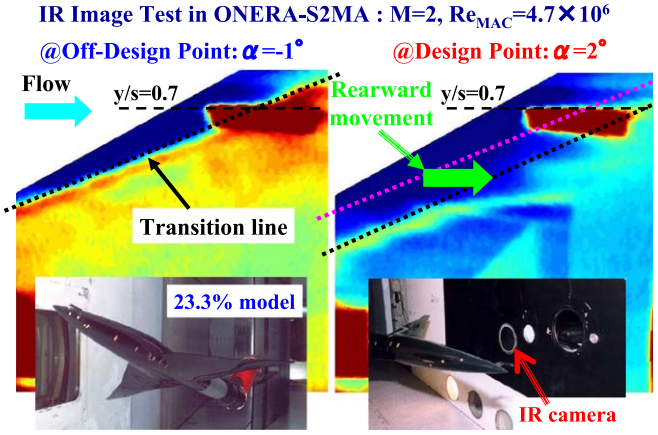

Fig. 18. Experimental validation test for transition characteristics.

aerodynamic configuration ("AS"), and the production shape manufactured using the jig was estimated assuming manufacturing process tolerances and 1G conditions. Then for each flight test condition, the aerodynamic loads were calculated and an elastically deformed shape ("ES") was estimated.

Furthermore, the real flight airplane includes some additional parts such as a camera, air data sensor (ADS), total temperature (TAT) sensor, and so on. A photograph of the final manufactured NEXST-1 vehicle is shown in Fig. 19.

3.2. Flight test results

3.2.1. Flight test conditions

In the flight test of the NEXST-1 airplane, two aerodynamic measurement phases were planned: an angle of attack (AOA) sweep test around 18 km altitude to obtain the airplane's drag characteristics, and an altitude sweep test while maintaining lift coefficient constant at the design value $C_L = 0.1$, corresponding to a Reynolds number (Re) sweep test, to investigate the effect of the NLF wing concept at higher Reynolds numbers than the design point. Since the NEXST-1 airplane was essentially a supersonic glider, it was impossible to precisely maintain the prescribed Mach number during the AOA sweep test, and a flight Mach number tolerance of 0.05 (namely from $M = 1.95$ to 2.05) was therefore specified considering wind tunnel test results [36].

The flight test was conducted at the Woomera test field in Australia on 10 October 2005. Fig. 20 shows the actual flight trajectory with photographs [37]. The achieved trajectory was almost exactly as predicted, with the vehicle well controlled by its onboard flight computer to realize the prescribed lift condition as shown in Fig. 21 [37].

During the AOA sweep phase, the flight altitude varied from 18.8 to 17.7 km corresponding to unit Reynolds numbers from 4.2 to 5.05 million, and the Reynolds number based on the mean aerodynamic chord (MAC) of 2.754 m varied from 12.4 to 14.6 million. Six AOAs were prescribed from -1.55° to 3.5°. The second, third, fourth, and fifth AOA values of -0.09°, 0.77°, 1.59°, and 2.54°, respectively, at which the measured lift coefficients C_L were 0.04, 0.07, 0.10, and 0.14, respectively. The design condition $C_L = 0.1$ was achieved at the fourth step.

During the Re sweep phase, the unit Reynolds number varied from 10 to 13.3 million corresponding to the variation of altitude from 12.1 to 11.5 km, and the Reynolds number based on MAC varied from 34.7 to 36.9 million. The AOA to maintain the constant $C_L = 0.1$ condition was around 1.7°. Although only a narrow Reynolds number range was achieved, the effect of Reynolds number sweep was investigated by comparing the result at the fourth step of the AOA sweep with the Re sweep test results.

3.2.2. Force characteristics

Force characteristics during the flight test were estimated using measured axial and normal accelerations $(\ddot{x},\ddot{z})$ or load factors referring to gravity $(N_x[G],N_z[G])$ and the following equations of force balance in a steady glide:

$$\begin{cases} A = W\sin\theta - m\ddot{x} \equiv -WN_x[G] \\ N = W\cos\theta - m\ddot{z} \equiv -WN_z[G] \end{cases} \tag{30}$$

where

$$\begin{cases} N_x[G] \equiv \frac{\ddot{x}}{g} - \sin\theta \\ N_z[G] \equiv \frac{\ddot{z}}{g} - \cos\theta \end{cases}$$

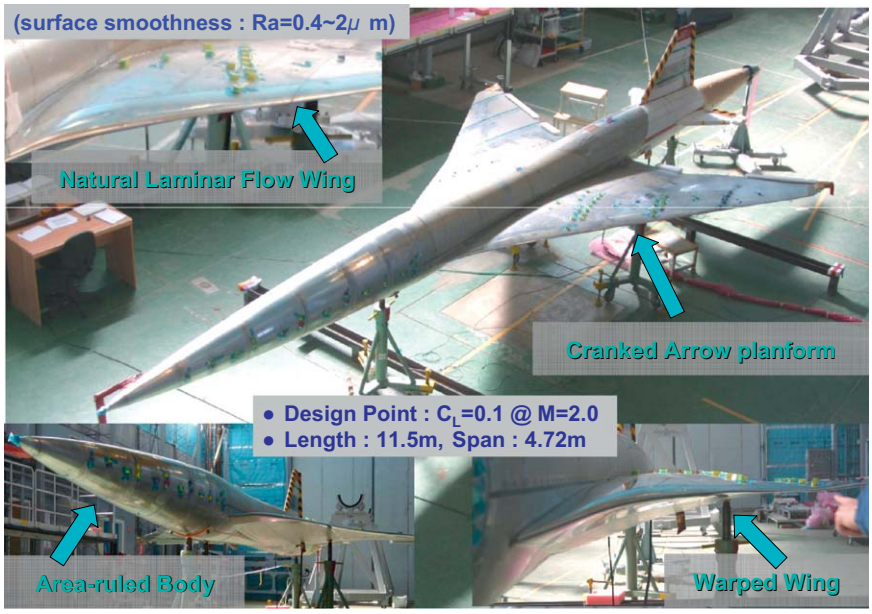

Fig. 19. Manufactured NEXST-1 airplane.

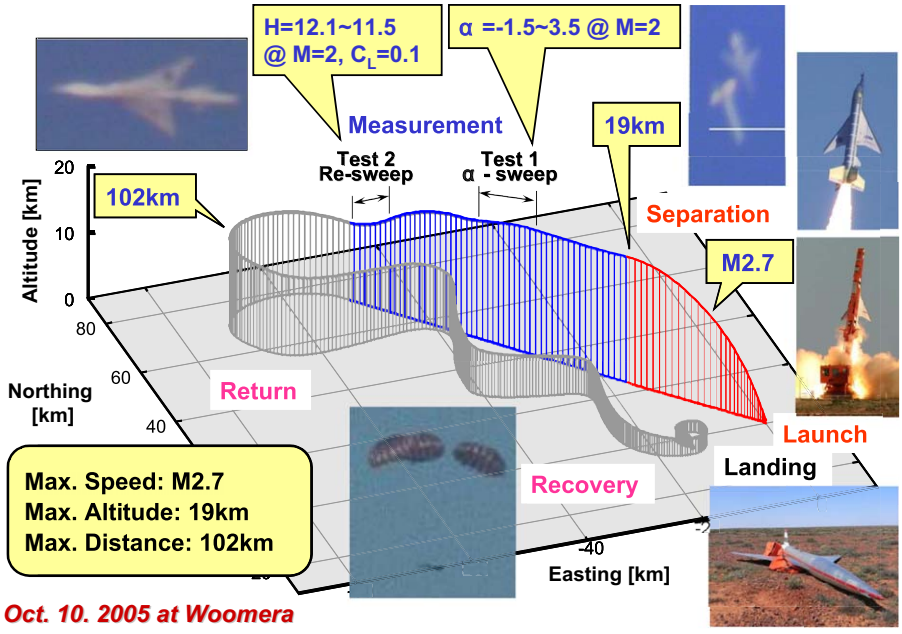

Fig. 20. Flight test results: flight trajectory.

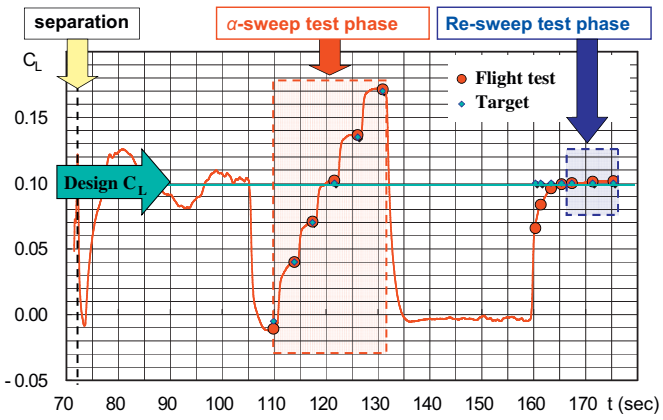

Fig. 21. Flight test results: comparison of measured and prescribed CL.

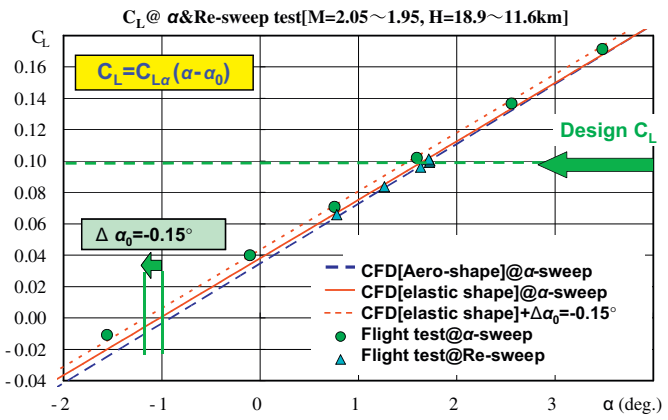

Fig. 22. Flight test results: lift characteristics.

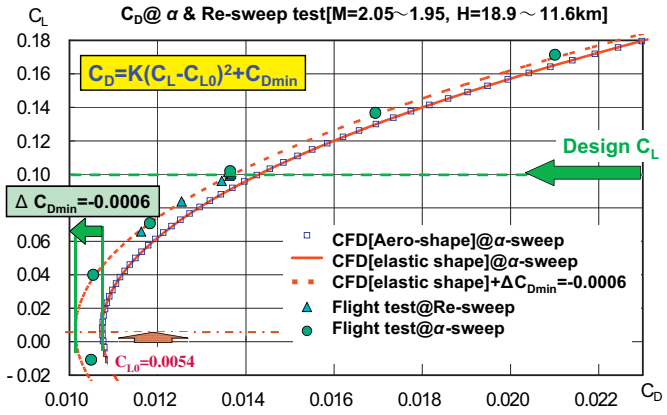

Fig. 23. Flight test results: drag characteristics.

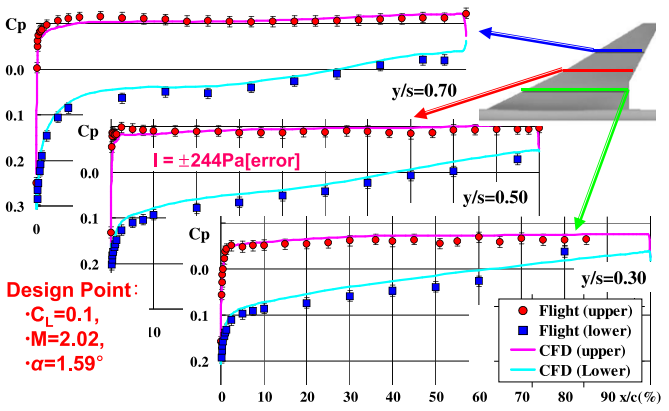

Fig. 24. Flight test results: pressure distributions on wing.

where A and N are the axial and normal aerodynamic forces, W and m are the weight and mass of the NEXST-1 airplane, and θ is the glide angle (i.e. the angle between the glide path and the horizontal plane). x and z are axes along the glide path and normal to it.

The lift and drag coefficients are easily calculated by the equations.

$$\begin{cases} C_L = \frac{L}{qS} = -\frac{W}{qS}(N_z \cos\alpha - N_x \sin\alpha) \\ C_D = \frac{D}{qS} = -\frac{W}{qS}(N_z \sin\alpha + N_x \cos\alpha) \end{cases} \quad (31)$$

Here the important parameters were as follows:

$W = mg = 1940.7\,\text{kg}$

$S = 10.12\,\text{m}^2$

where m is the measured mass of the airplane.

Fig. 22 compares the flight test lift data indicated by solid symbols with CFD predictions for the AS and ES. The flight test lift slope $C_{L\alpha}$ value agrees well with the CFD result considering elastic deformation of the wing [38]. However, the measured zero-lift angle α_0 is slightly different from the CFD analysis, by about 0.15°. The reason for this discrepancy has not been clarified.

The drag characteristics are summarized in Fig. 23, comparing the flight test data with CFD predictions for the AS and ES. The CFD drag polar curves of the AS and ES are almost identical. As is easily seen in the figure, except for $C_{D\min}$ the measured K and C_{L0} values agree well with CFD predictions, confirming the arrow planform and warped wing concepts. On the other hand, the remarkable difference in $C_{D\min}$ does not validate the area-ruled body concept. This discrepancy might be explained by the fact that the minimum drag of the NEXST-1 airplane was increased by additional parts such as ADS, TAT, camera, etc. and elastic deformation, and by the fact that the CFD analysis had an error in the turbulence model used to estimate friction drag [38–41]. The effect of the area-ruled body concept could not therefore be directly confirmed from measured drag characteristics.

3.2.3. Pressure distributions

The pressure distributions on the wing and body surfaces were measured by about 330 pressure taps. The pressure measurement system had a response delay due to the length of tubing between the taps and detection modules. The time interval to compensate this delay was found in preliminary tests, and was applied to each AOA step to obtain constant Cp conditions [42].

Fig. 24 compares the measured and computed pressure coefficient (Cp) distributions on the wing at the design condition, namely at the fourth AOA sweep. These computed

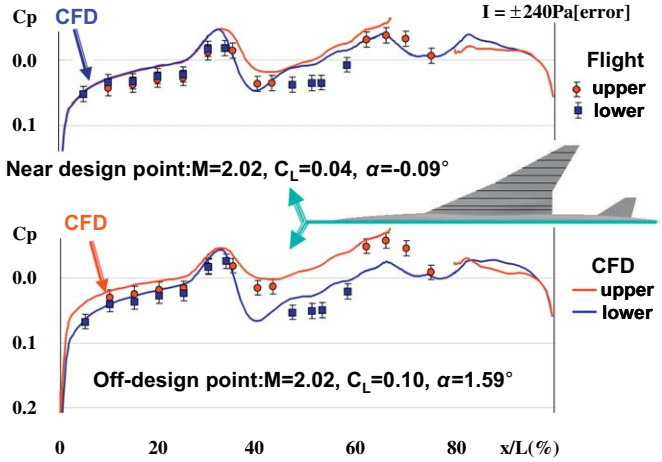

Fig. 25. Flight test results: pressure distributions on fuselage.

results are for the AS. Good agreement of the upper Cp distributions is confirmed within the 244 Pa error bar of the measurement system [42]. This means the necessary condition for the NLF wing was satisfied in the flight test. However, a slight difference in the lower surface Cp distributions between the flight test and prediction is recognised, and this difference is also found in with CFD predictions for the ES. The reason for this has not yet been clarified.

Fig. 25 compares the measured and predicted pressure coefficient distributions on the fuselage centre section at near design point and off-design point flight test conditions, namely the second and fourth AOA sweeps. A fairly good qualitative agreement in the Cp distributions is confirmed, but there is a clear quantitative difference between the flight test and CFD data. We suppose that the principal reason for this is the non-smoothness of curvature of each panel that formed the fuselage contour. However, we consider that the qualitative agreement indirectly confirms our area-ruled body concept.

3.2.4. Transition characteristics

As an example of transition detection sensor measurements, Fig. 26 shows time histories of the DC (E_MEAN) and AC (e'_RMS) signal components from a hot-film sensor located on the surface of the inner wing. In general, a higher DC level indicates that the boundary layer is turbulent, while the AC level is lower in laminar flow, maximum at transition, and higher than the laminar level in

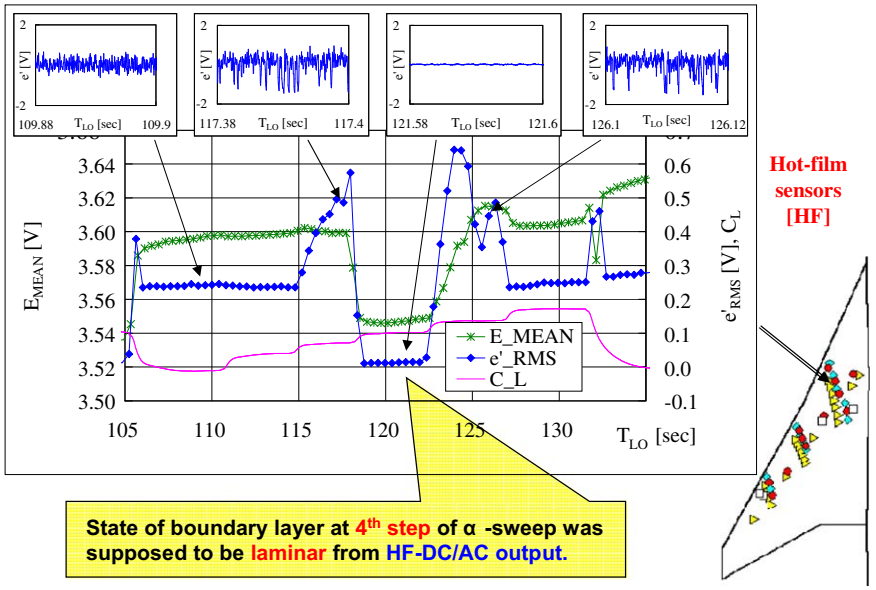

Fig. 26. Flight test results: time history of hot-film (HF) signals.

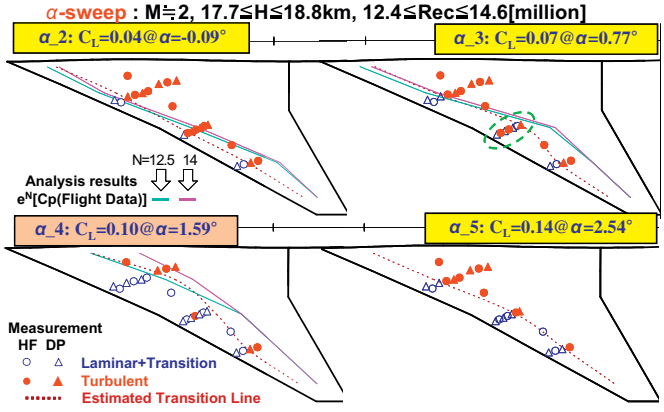

Fig. 27. Flight test results: measured transition locations at AOA-sweep test phase.

turbulent flow. A laminar boundary layer is clearly demonstrated by both DC and AC levels in the time interval 118–122 s, which corresponds to the design lift condition, namely the fourth AOA sweep.

In order to analyze the transition data precisely, the state of the boundary layer was classified by a newly introduced transition level criterion based on sensor AC output [43–45]. Transition levels range from 1 (fully laminar) to 7 (fully turbulent), with the transition process occupying levels 2–6. The estimated "end of transition" line indicating the boundary between non-turbulent and turbulent regions is the supposed boundary between levels 5 and 6.

Fig. 27 compares the transition characteristics predicted by analysis and the turbulent and non-turbulent areas measured during the AOA sweep. The rearward movement of the boundary between turbulent and non-turbulent regions, namely about 40% local chordwise location at the design AOA condition is confirmed. However, there are inconsistencies between the results from HF and DP sensors in the mid-wing region for reasons which are not yet clear.

In the Re sweep test, the expected significant rearward movement of the boundary was not observed. While the reason is still not clear, we speculate that surface roughness is the primary cause since the measured roughness of 1 μm for the "Ra-metric" is much greater than the target level of 0.3 μm. Again, an inconsistency between detections using HF and DP sensors in the mid-wing region is observed, the cause of which is not yet clear.

In addition, no transition due to attachment-line contamination was apparent in the Re sweep test. This is probably good evidence that the forwardmost sensors at the 15% chordwise position at each spanwise station detected a laminar state, unless relaminarisation occurred off the attachment-line, but this has not yet been fully confirmed.

3.2.5. *Summary of flight test results*

The flight test results can be summarized as follows. The effects of the arrow planform and warped wing concepts were validated directly by the close agreement of the flight test measurements of $C_{L\alpha}$, K, C_{L0} and their CFD-predicted values. The effect of the NLF wing design concept was validated by the good agreement of Cp distributions on the wing between the test data and CFD analysis, and the rearward movement of the transition location at the design condition. The measured laminar region is supposed to be about 40% of the upper wing surface. Furthermore, good agreement of fuselage Cp distribution between the test data and CFD analysis probably validates the effect of the area-ruled design concept; however, a discrepancy between the measured and predicted $C_{D\min}$ meant that it was difficult to validate the effect of the NLF wing design concept quantitatively by the flight test, because it is difficult to estimate turbulent skin friction reliably by any turbulence model.

It can be concluded that the flight test proved our drag reduction concepts. However, the effect of Reynolds number variation was not completely obtained.

3.2.6. *Comparison of transition prediction method with measured transition data*

Predicting transition is generally one of the most challenging subjects in aerodynamics. In the NEXST-1 project, a new NLF wing design concept was devised, and JAXA developed a new transition prediction method based on the current e^N method. This method requires a threshold value of N to be set to predict the transition. Before the NEXST-1 flight test, a value of $N = 14$ was applied, referring to Ref. [31]. After the flight test, the N threshold value for

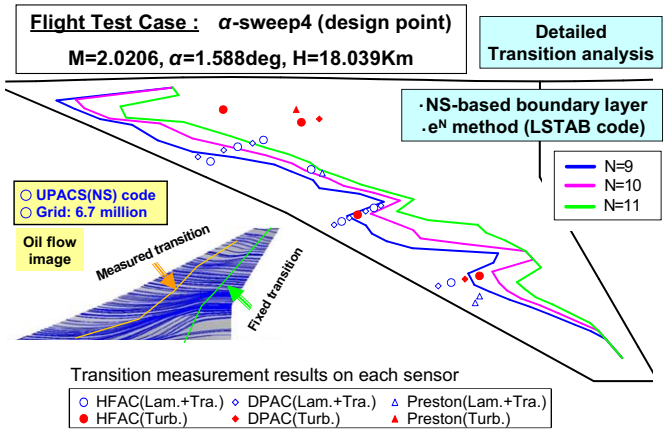

Fig. 28. Comparison of measured results with detailed transition analysis results.

Table 2
Evaluation of NEXST-1 aerodynamic design technology.

Design point: $M = 2$, $C_L = 0.1$, $H = 18.3$ km	1st Gen. SST	NEXST-1 technology	
	Reference type	NEXST-1 airplane	Full-size SST
Length (m)	62.0	11.5	91.4
Wing area (m^2)	412.2	10.1	836.1
Aspect ratio	1.6	2.2	2.2
M.A.C. (m)	21.6	2.8	25.0
Re_{MAC} (10^6)	104.0	13.9	120.6
Laminarization at upper wing (%)	0	40	30
Friction drag	0.00463	0.00602	0.00421
Pressure drag	0.00818	0.00768	0.00714
Total drag	0.01281	0.01370	0.01135
L/D at design point	7.81	7.30	8.81
Improvement rate (%)	0	−6.5	12.9

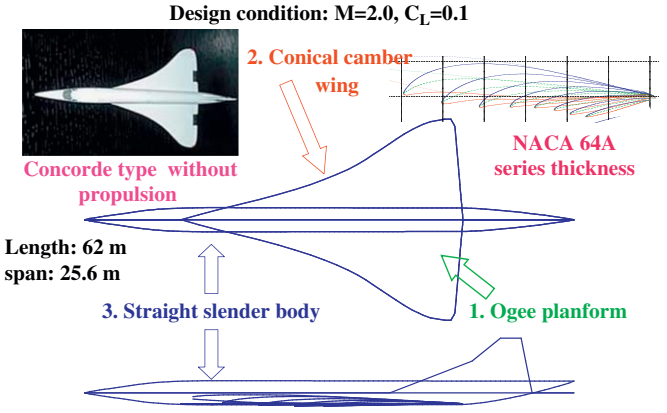

Fig. 29. Design concepts of 1st generation SST.

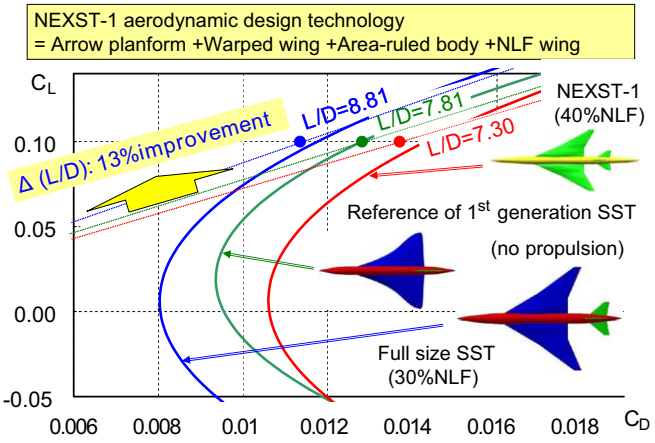

Fig. 30. Estimated effect on full-size SST.

the flight conditions was expected to be determined by comparing the predicted N contours with the measured transition characteristics.

However, a more precise analysis of laminar boundary layer characteristics under the flight test conditions was conducted using a Navier–Stokes code assuming a laminar boundary layer on the wing surface from the leading edge to 80% of local chord. The transition N patterns estimated from present NS-based boundary layer characteristics are shown in Fig. 28, compared with flight measurements from the transition detection sensors. Although against our expectation no constant values of N were found, the $N = 11$ contour shows good correlation with the flight data over the inner wing [33].

The discrepancy between the NS-based prediction and flight test data is supposed to be largely due to surface roughness; that is, it is thought that the surface of the NEXST-1 airplane's wing was not sufficiently smooth because of the lack of a pronounced transition delay at higher Reynolds numbers that be expected from a smooth surface. Investigations into this matter are continuing.

3.3. *Evaluation of aerodynamic design effects*

Along with the validation of its NEXST-1 aerodynamic design concepts, JAXA investigated the overall effectiveness of applying these concepts to a full-size SST configuration by comparing the effect of the NEXST-1 concepts with a representative "Reference" configuration corresponding to a first generation SST.

For this comparison, we designed two full-scale SSTs based on the dimensions mentioned above: the Reference configuration (a Concorde-like configuration without nacelles) using current aerodynamic design practices referring to [8], which are summarized in Fig. 29, and a full-scale configuration using NEXST-1 concepts. For the latter, it was predicted that the 40% laminarization achieved on the upper surface of the NEXST-1 airplane demonstrated by the flight test would actually be a 30% laminarization for a full-scale configuration if a new optimum pressure distribution for the NLF wing design at a higher Reynolds number condition were applied.

The principal results of this comparison are summarized in Table 2 and Fig. 30. Applying the NEXST-1 design concepts improves the L/D by about 13% at the cruise condition compared with the Reference configuration shown in Table 2, and improvement is also evident in the predicted drag polar curves shown in Fig. 30.

4. Further works in JAXA supersonic research program

4.1. *Aerodynamic design of jet-powered scaled supersonic experimental airplane*

The NEXST-2 program using a jet-powered experimental airplane is the second step of JAXA's plan to develop advanced design technologies. The main emphasis of this program is placed on reducing supersonic drag due to interference between the airframe and propulsion system, as well as subsonic drag

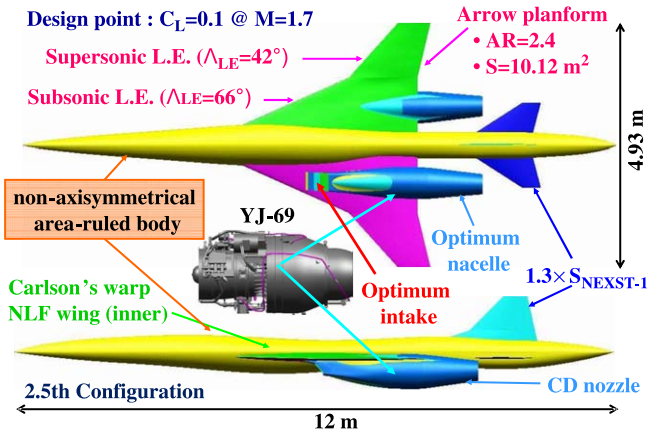

Fig. 31. NEXST-2 aerodynamic design concepts [23].

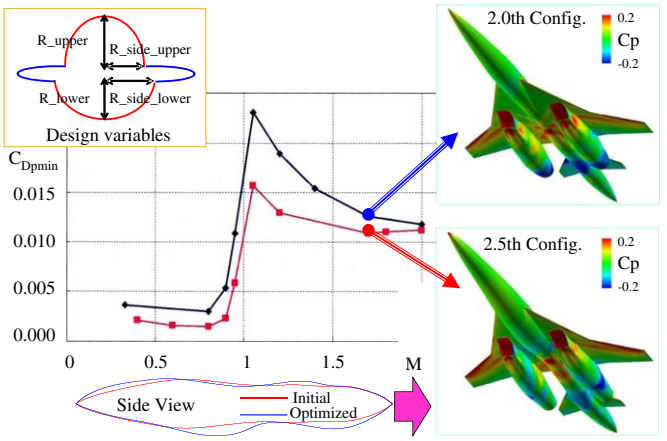

Fig. 32. Effect of non-axisymmetric area-ruled body concept in the NEXST-2 airplane.

reduction. The Teledyne YJ69 engine was selected considering cost constraints and its ready availability [1,23,27].

The NEXST-2 airplane has two large nacelles covering the engines. The nacelles have a larger maximum diameter than that of fuselage, and so reduction of interference drag between the airframe and nacelles is strongly required. This made the NEXST-2 design a good platform for developing an interference drag reduction concept. JAXA developed an original CFD-based optimum design method [23,46,47], and an optimum intake was also designed using several fundamental results from both wind tunnel tests and CFD-based analysis [48–52]. These design concepts, processes and results are briefly outlined in the following sections.

4.1.1. Design concepts

The NEXST-2 airplane was designed for Mach number of 1.7 in consideration of engine performance. Its dimensions are similar to the NEXST-1 airplane. The NEXST-2 design concepts are summarized in Fig. 31, and consist of concepts applied to the NEXST-1 airplane design and some new concepts developed for the NEXST-2 program.

4.1.1.1. NEXST-1 design concepts [23]. To improve the airplane's subsonic aerodynamics, a modified arrow planform with an aspect ratio of 2.4, 0.2 greater than that of the NEXST-1 airplane, was selected. As the increase in aspect ratio reduced the sweep angle of the outer wing, the outer wing has a supersonic leading edge, and a sharp leading edge section was adopted to reduce the wave drag due to bow shock that originates from a rounded leading edge.

Using linear theory it is generally difficult to incorporate the influence of shock waves due to the nacelles in the design. Therefore, a warped wing was designed omitting the nacelles at a reduced design C_L. A CFD computation of the NEXST-2 baseline configuration showed C_L increase of 0.06 due to compression lift generated by interference between the nacelles and wing. As the total design lift coefficient was 0.1, the reduced design C_L for the warp design was estimated to be 0.04.

The NLF wing concept was applied only to the inner wing. Since the concept for suppressing C–F instability requires a rounded leading edge, it could not be applied to the outer wing with its sharp leading edge. The target pressure distribution was derived considering the computed pressure levels on the NEXST-2 baseline configuration at the reduced design condition (namely $C_L = 0.04$) and setting the distribution shape to be that of the target pressure distribution of the NEXST-1 airplane. Although geometry modification was applied only to the inner wing at each iteration of the CFD-based inverse design procedure, CFD analysis was conducted for the complete configuration including nacelles.

4.1.1.2. New design concepts for the NEXST-2 airplane [23]. The chief difference between the NEXST-1 and the NEXST-2 airplane design processes was mainly to consider the influences of intakes, nacelles, diverters, and the internal flow effects of the nacelles. The NEXST-2 design process is summarized below.

The general principle applied to reduce interference drag between the airframe and nacelles was to decrease the cross-sectional area of total configuration. One of the best ways to achieve this is to embed the nacelles into the wing as far structural constraints allow.

It was difficult to apply the axisymmetrical area-ruled body concept to the NEXST-2 design because of overriding constraints on minimum diameter, minimum volume and maximum length. Moreover, as mentioned above, the linear theory-based area-ruled body concept cannot handle the influences of shocks and expansion waves due to the intakes and nacelles. It was therefore needed to expand the area-ruled body concept to include nonlinear effects, and so JAXA developed an original CFD-based optimum design method and a non-axisymmetrical area-ruled body design concept to reduce interference drag between airframe and nacelles [46]. Since the geometry of the lower fuselage is dominant in controlling drag due to interference between the airframe and nacelles, the key point of the concept is to optimize the upper and lower fuselage geometries independently using a certain mathematical formulation of two kinds of radial distributions as design variables, as shown in Fig. 32.

The principle of the method is to design an optimum configuration by analyzing the sensitivity of design variables on total pressure drag chosen as an objective function. The method consists of an Euler solver with an overset grid system for calculating flow characteristics and an adjoint method for analyzing sensitivity of geometry on flow quantities [46,47]. The adjoint method used is known to be very effective for reducing CPU time of Euler calculations. Furthermore, the overset grid was also very effective for optimizing a complex wing–body configuration with such large nacelles. However, the results of the method strongly depend upon the initial configuration, and so this had to be carefully designed using the aerodynamic design techniques employed for the NEXST-1 airplane.

The optimum nacelle configuration and position, such as the streamwise station and spacing of the nacelles, were also determined using the CFD-based optimum design method [47]. The shapes of the external compression type intake and convergence–divergence (CD) nozzle were designed using CFD

analysis and an experimental database compiled by JAXA. These research activities are summarized in Refs. [48–52].

Attention was then turned to improving the precision of the flowfield analysis around the NEXST-2 airplane, considering how to simulate the operating conditions of the engines; that is, how to estimate the inflow into the intakes and outflow from the nozzles as precisely as possible. In general, the flowfield around a vehicle is analyzed using a so-called flow-through-nacelle condition as an approximation. Confirming the validity of this approximation was one of the targets for the development of the NEXST-2 airplane design techniques.

4.1.2. Design process and results

The aerodynamic design process of the NEXST-2 airplane consisted of two phases. First was a conceptual design phase with the objective of achieving an aerodynamic design that compromises between constraints such as wing position, aerodynamic tail volume, intake geometry, the configuration of the front part of the nacelles, and the embedded nacelle condition. This was followed by an aerodynamic optimum design phase, which focused on the non-axisymmetrical area-ruled body design, including the optimum nacelle design. The results of each of phase are described below [23].

4.1.2.1. Conceptual design phase. As a first step, JAXA designed a baseline configuration with two large nacelles. This configuration had a simple straight body with a Von Kármán ogive cone and a warped wing derived by Carlson's method. The planform was selected considering drag characteristics estimated using Carlson's method according to the same selection rules as the NEXST-1 airplane. The chief difference was the adoption of a supersonic leading edge for the outer wing as mentioned above. This configuration was called "0–1st Configuration", shown in Fig. 34, and was used in wind tunnel tests [53] to investigate low-speed and transonic aerodynamic characteristics and nacelle flow effects in supersonic flow as well as supersonic aerodynamics.

Following this, JAXA then designed further configurations from the 0–2nd Configuration to the 0–8th Configuration using linear theory-based design methods with improvements to the configuration and position of the nacelles, and optimization of intake geometry and aerodynamic tail volume. This design process was not straightforward but was largely a trial and error approach for reducing aerodynamic drag while considering several practical constraints. The final conceptual configuration called "0–8th" is shown in Fig. 33.

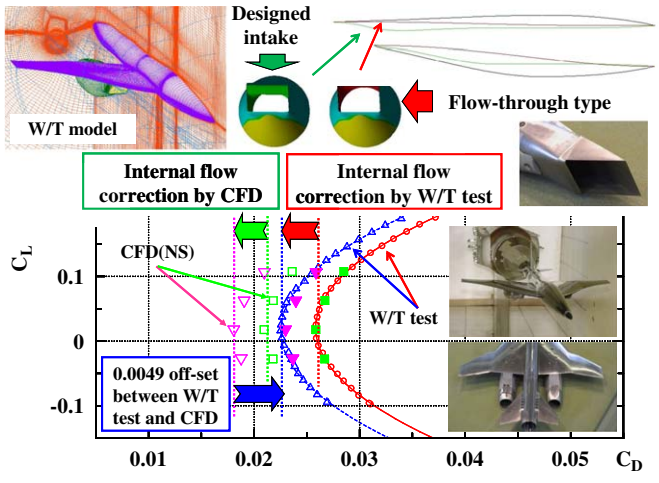

Fig. 33. Wind tunnel test results for CFD validation [23,54].

4.1.2.2. Aerodynamic optimum design phase. In order to develop a practical experimental airplane, it was necessary to compromise between airframe aerodynamics, structural constraints, flight dynamics, intake aerodynamics, and propulsion system performance. JAXA designed a "1st Configuration" using the new CFD-based aerodynamic design method and considering several of these practical constraints. The initial configuration for this process was the 0–8th Configuration from the conceptual design phase.

The 1st Configuration was submitted to industrial partners who examined it from several viewpoints, and from this the following new requirements emerged: a 0.5 m extension of the fuselage, greater fuel capacity, an increase of thickness ratio from $t/c = 3\%$ to 5%, an increase in fuselage diameter by about 2 in, enlargement of the nacelle diameter by 0.1 m, and a clearance of 0.015 m between the nacelle and lower surface of the wing at front of the diverter. Furthermore, the pressure drag of the configuration near sonic speed had to be drastically reduced. Therefore, reducing the drag over the whole Mach number range was set as the most important target for the subsequent design iteration.

In the aerodynamic design of an improved configuration derived from the 1st Configuration, the NLF wing from the previous configuration was adopted without modification and the optimum nacelle position was applied. The non-axisymmetrical fuselage design concept was also applied. The resulting configuration was called "2.0th Configuration".

Furthermore, in order to reduce interference drag near sonic speed, a new optimum non-axisymmetrical area-ruled body was designed using a different initial configuration with a similar area distribution to that of the 0–7th Configuration, because this had been found to have the best potential to reduce interference drag from transonic to low supersonic speed. The resulting configuration was called the "2.5th Configuration". Finally, the minimum pressure drag characteristics were estimated over the whole Mach number range as shown in Fig. 32, which showed that the desired effect had been achieved. Consequently, the 2.5th Configuration was selected as the final aerodynamic configuration for the NEXST-2 airplane.

4.1.3. Wind tunnel tests

Several wind tunnel tests were conducted to completely understand the airframe/nacelle interference and to develop a reliable and effective database for the supersonic intake [48–52]. The principal results of these fundamental research activities except the intake tests are summarized below.

4.1.3.1. CFD validation tests of the airframe/nacelle interference configuration model. A flow-through-nacelle wind tunnel model of the 0–8th Configuration was used to validate the CFD results for a complex configuration with nacelles. Fig. 33 shows the 8.3% scale force test model with a modified intake shape and a CFD grid. Both supersonic and subsonic tests were conducted at JAXA [34,54].

Fig. 33 shows the measured and corrected drag polar curves compared with CFD (NS) computation results. In flow-through-nacelle tests, the drag measured by a force balance should be corrected using the momentum balance of the internal flow of the nacelle, and the open circle and triangle symbols indicate measured drag characteristics without and with this correction, respectively. The CFD-computed drag is somewhat lower than the measured characteristics both with and without internal flow correction, but depends strongly on the CFD turbulence model. If computed drag characteristics with an offset value 0.0049 of the minimum drag are assumed, very high correlation is found with the wind tunnel test results. Therefore, the pressure drag characteristics estimated by the CFD code were considered to be well validated.

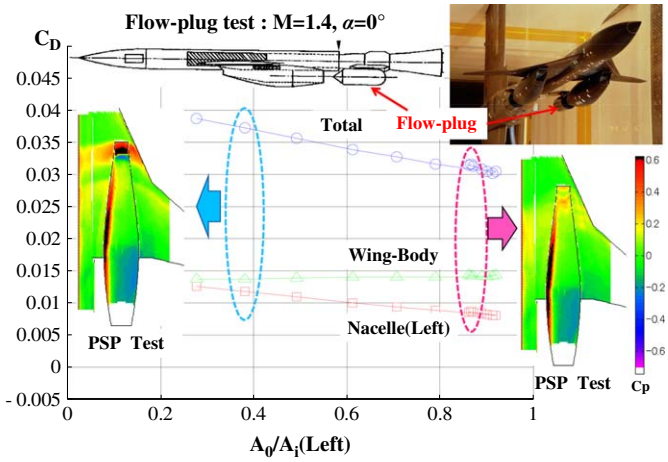

Fig. 34. Wind tunnel test results for nacelle flow effect [23,53].

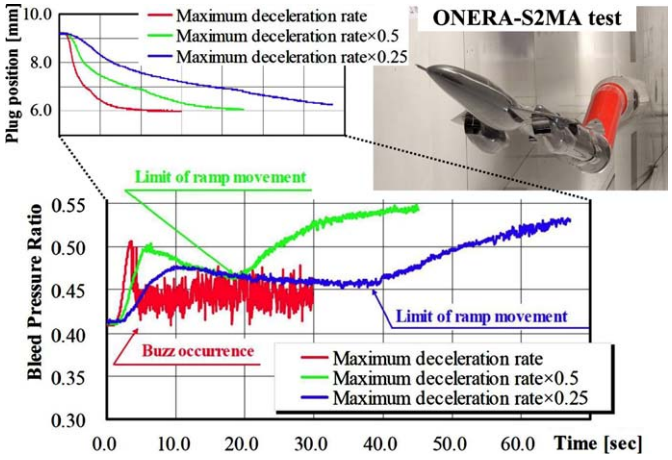

Fig. 35. Effect of engine deceleration rate on bleed pressure ratio [51].

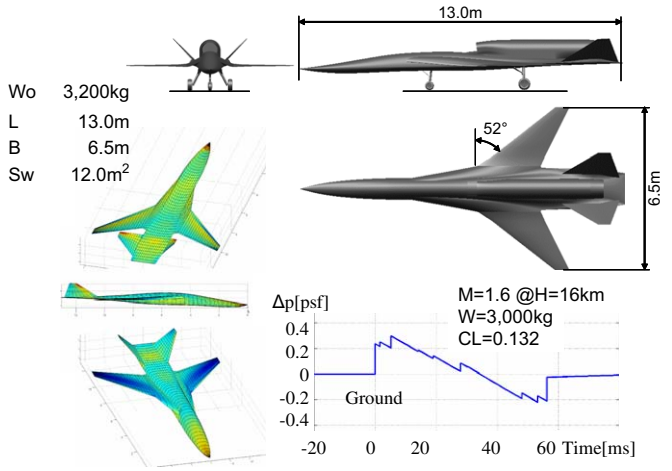

Fig. 36. S3TD baseline configuration designed with CAPAS [3].

4.1.3.2. Flow-plug tests for the nacelle flow effect on drag characteristics. In order to collect complete NEXST-2 airplane drag data for the system design phase, the mass flow effect of the nacelles on airframe drag characteristics was investigated. For this purpose, a slightly larger test model (17.0% scale) of the 0–1st Configuration with two flow control plugs behind each nacelle was constructed as shown in Fig. 34, and a flow-plug test was carried out in JAXA's 2 m × 2 m transonic wind tunnel [53].

Fig. 34 shows how drag characteristics vary with nacelle mass flow ratio (*A*0/*Ai*) at Mach 1.4. Here, *A*0 and *Ai* indicate the cross-sectional area of actual flow stream tube at forward infinity and the capture area at the front of the intake. The figure indicates an increase in nacelle drag as the mass flow ratio decreases, and that the total drag depends strongly on nacelle drag. Fig. 34 shows pressure distributions measured by pressure sensitive paint (PSP) technique [55] for two typical cases of small and large values of *A*0/*Ai*. The PSP reveals a strong shock wave in front of the intake in the low mass–flow ratio condition, a flow pattern which corresponds to the "unstart" condition. On the other hand, with a high mass flow ratio there is no remarkable shock wave in front of the nacelle.

4.1.3.3. Supersonic intake performance tests. Supersonic intake performance was investigated in detail in the ONERA-S2MA facility for Mach numbers from 1.5 to 2.9 using a 15% scale fuselage, inboard wing and nacelles model of the 2.5th Configuration [51]. A sample test result, the effect of engine deceleration rate on bleed pressure ratio, is shown in Fig. 35. In order to clarify engine operation requirements, three rates of the engine deceleration were examined. "Buzz" occurred at the fastest rate, labeled "Maximum deceleration rate" in the figure, and stable intake operation was never recovered. For the slowest engine deceleration rate, namely "Maximum deceleration rate × 0.25", the bleed pressure ratio was maintained at almost a constant value and buzz was successfully avoided. Consequently, the engines should be operated at a rate at least as slow as quarter of the maximum rate used in the test to achieve stable intake operation.

4.2. Outline of silent supersonic technology demonstration program

Sonic boom is one of the biggest problems that must be addressed to allow supersonic flight over land. Following on from the NEXST program, JAXA initiated the "Silent Supersonic Technology Demonstration" program in 2006 with a target of reducing sonic boom intensity by 50% [3]. The program will validate design tools such as a multi-disciplinary optimization design tool and demonstrate silent supersonic technologies such as a low-boom/low-drag configuration design methodology and low-noise nozzle concepts by a Silent Supersonic Technology Demonstrator "S3TD".

In general, current low-boom design methods generally lead to configurations with a blunt nose and rear-lifting-body, which increases wave drag due to volume, and require a certain airframe cross-sectional area distribution, which cannot be satisfied by an area-ruled body design and also generates stability problems such as trim problems. Therefore, the main objective of an advanced aerodynamic design technique for silent supersonic aircraft is not only to reduce sonic boom intensity but also to maintain low drag equivalent to a high *L*/*D* design.

The first key concept for the design technique is to apply the non-axisymmetrical area-ruled body design method [46] to reduce the drag due to the blunt nose and non-area-ruled body of the low-boom configuration [56]. The second concept is to use multi-objective optimization combined with a genetic algorithm (GA) technique. The GA technique is very powerful tool for finding configurations that optimize multiple objectives—for example, minimizing sonic boom intensity, increasing *L*/*D* at both supersonic and subsonic speeds, reducing weight, etc.—but requires much computation time. As a first step towards the development of practical tools, JAXA has developed a "CAD-based Automatic Panel Analysis System (CAPAS)" design tool based on linear theory and applied it to the design of the S3TD baseline configuration [57].

Fig. 36 shows the outline of the S3TD baseline configuration and its estimated sonic boom signature on the ground [3]. An upper-mounted engine was required to reduce engine noise and to shield against shock waves from the intake. A remarkable nose configuration was designed by optimizing design variables characterizing the fuselage configuration to reduce both pressure drag and the front pressure rise of the boom on the ground. A rear flat-deck was also designed to realize both the rearward lift required by low-boom theory and to achieve trim in cruise conditions. Furthermore, the intake on the upper fuselage was carefully designed using some useful results from the NEXST program. Presently JAXA is currently engaged in design studies of a more detailed configuration [57].

5. Concluding remarks

JAXA has developed CFD-based supersonic drag reduction techniques through fundamental research for its NEXST unmanned-scaled supersonic flight experiment program, and has further developed the techniques in research for the follow-on S3TD project.

A supersonic NLF wing design concept and a CFD-based inverse design procedure were newly developed for the first NEXST airplane, and a non-axisymmetrical area-ruled body concept and a CFD-based optimum design procedure were developed for the second NEXST airplane. The NLF wing concept was first validated qualitatively by tests at the ONERA-S2MA wind tunnel test that has low inherent freestream turbulence. Flight tests then confirmed that NLF wing design delayed actual transition to about 40% local chord, although this was earlier than the pre-flight prediction by JAXA's transition prediction tool based on current e^N methods.

The NEXST-1 aerodynamic design techniques were validated through the analysis of flight test data, and were estimated to achieve an L/D about 13% greater than could be attained by conventional design methods for a 1st generation SST.

To reduce the strong interference drag between the airframe and two large nacelles of the second NEXST airplane, the effect of the non-axisymmetrical area-ruled body concept was confirmed numerically. The concept has not been validated experimentally because it is not easy to simulate the complete flowfield around a complex configuration with engines in an operating condition in wind tunnel tests. Therefore, JAXA has promoted several fundamental research activities relating to those challenging issues.

Finally, flight test of the S3TD demonstrator are strongly desired to establish all the design techniques developed by JAXA.

Acknowledgments

The author would like to express special thanks to Mitsubishi Heavy Industries (MHI), Kawasaki Heavy Industries (KHI), Fuji Heavy Industries (FHI) and Tohoku University for their cooperation in the aerodynamic designs of both NEXST airplanes. In addition, many research activities related to those designs were supported by several JAXA researchers, and the author would like to thank them also.

References

[1] Sakata K. Supersonic Research Program in NAL, Japan. In: First international CFD workshop for super-sonic transport design, Tokyo, March 1998, p. 1–4.
[2] Ohnuki T, Hirako K, Sakata K. National Experimental Supersonic Transport Project. ICAS2006-1.4.1, 25th ICAS, Hamburg, September 2006.
[3] Murakami A. Silent Supersonic Technology Demonstration Program. ICAS2006, 25th ICAS, Hamburg, September 2006.
[4] Hanai T, Yoshida K, Usuki K, Tamaki T. Research trend in supersonic transport. Journal of the Japan Society for Aeronautics and Space Sciences 1989;37(430):1–13 [in Japanese].
[5] Society of Japanese Aerospace Companies (SJAC). Development trend study of supersonic transport (annual report). 1993 [in Japanese].
[6] Yoshida K. Fundamental research topics on aerodynamic shape of SST-based on in-house research reports. Journal of the Japan Society for Aeronautics and Space Sciences 1994;42(486):1–13 [in Japanese].
[7] Kuchemann D. The aerodynamic design of aircraft. Pergamon Press; 1978.
[8] Rech J, Leyman CS. A case study by Aerospatiale and British Aerospace on the Concorde. AIAA Professional Study Series, 1981.
[9] Corning G. Supersonic and subsonic, CTOL and VTOL, Airplane design, 4th ed. Maryland, 1976.
[10] Jones RT. Theoretical determination of the minimum drag of airfoils at supersonic speeds. Journal of Aeronautical Sciences 1952;19:813–22.
[11] Ashley H, Landahl M. Aerodynamics of wings and bodies. Dover Publications Inc.; 1965.
[12] Arnal D. Boundary layer transition prediction based on linear theory. AGARD report 793, 1993.
[13] Smith JHB, Mangler KW. The use of conical camber to produce flow attachment at the leading edge of a delta wing and to minimize lift-dependent drag at sonic and supersonic speeds. A.R.C. R&M no. 3289, 1957.
[14] Smith JHB, Beasley JA. The calculation of the warp to produce a given load and the pressure due to a given thickness on thin slender wings in supersonic flow. A.R.C. R&M no.3471, 1967.
[15] Carlson HW, Middleton WD. A numerical method for the design of camber surfaces of supersonic wings with arbitrary planforms. NASA TN D-2341, 1964.
[16] Carlson HW, Miller DS. Numerical method for the design and analysis of wings at supersonic speeds. NASA TN D-7713, 1974.
[17] Ogoshi H. Aerodynamic design of a supersonic airplane wing-application of the natural laminar flow concept to airfoil. In: Proceedings of the 47th national congress of theoretical & applied mechanics, January 1998 [in Japanese].
[18] Srokowski AJ. Mass flow requirement for LFC wing design, AIAA-77-1222, 1977.
[19] Matsushima K, Iwamiya T, Nakahashi K. Wing design for supersonic transports using integral equation method. Engineering Analysis with Boundary Elements 2004;28:247–55.
[20] Matsushima K, Iwamiya T, Ishikawa H. Supersonic inverse design of wings for the full configuration of Japanese SST. ICAS2000, 2000, p. 213.
[21] Jeong S, Matsushima K, Iwamiya T, Obayashi S, Nakahashi K. Inverse design method for wings of supersonic transport. AIAA 98-0602, 1998.
[22] Yates JE, Donaldson CA. Fundamental study of drag and an assessment of conventional drag-due-to-lift reduction devices. NASA CR 4004, 1986.
[23] Yoshida K, Makino Y. Aerodynamic design of unmanned and scaled supersonic experimental airplane in Japan, ECCOMAS 2004, Jyväskylä, July 2004.
[24] Boeing Commercial Airplanes. High-Speed Civil Transport Study. NASA CR-4233, 1989.
[25] Douglas Aircraft Company. Study of high-speed civil transports. NASA CR-4235, 1989.
[26] Takaki R, Iwamiya T, Aoki A. CFD analysis applied to the supersonic research airplane. In: First international CFD workshop on supersonic transport design, Tokyo, March 1998.
[27] Yoshida K. Overview of NAL's program including the aerodynamic design of the scaled supersonic airplane. Held at the VKI, RTO Educational Notes 4, 15-1–16, 1998.
[28] Shimbo Y, Yoshida K, Iwamiya T, Takaki R, Matsushima K. aerodynamic design of the scaled supersonic experimental airplane. In: First international CFD workshop for super-sonic transport design, Tokyo, March 1998.
[29] Middleton WD, Lundry JL. A system for aerodynamic design and analysis of supersonic aircraft. NASA Contractor report 3351, 1980.
[30] Yoshida K, Ishida Y, Noguchi M, Ogoshi H, Inagaki K. Experimental and numerical analysis of laminar flow control at Mach 1.4. AIAA 99-3655, 1999.
[31] Joslin RD. Aircraft laminar flow control. Annual Review of Fluid Mechanics 1998;30:1–20.
[32] Poll DIA. Boundary layer transition on the windward face of space shuttle during re-entry. AIAA paper 85-0899, 1995.
[33] Yoshida K, Sugiura H, Ueda Y, Ishikawa H, Tokugawa N, Atobe T, et al. Experimental and numerical research on boundary layer transition analysis at supersonic speed: JAXA-ONERA cooperative research project. JAXA-RR-08-007E [to be published].
[34] Yoshida K, Makino Y, Shimbo Y. An experimental study on unmanned scaled supersonic experimental airplane. AIAA-2002-2842, 2002.
[35] Sugiura H, Yoshida K, Tokugawa N, Takagi S, Nishizawa A. Transition measurements on the natural laminar flow wing at Mach 2. Journal of Aircraft 2002;39(6):996–1002.
[36] Machida S, Yoshida K, Ohnuki T. Supersonic flight testing of unmanned experimental airplane for next-generation SST. AIAA-2007-854, 2007.
[37] Fujiwara T, Hirako K, Ohnuki T. Flight plan and flight test results of experimental SST vehicle NEXST-1. ICAS2006-6.2.1, 25th ICAS, Hamburg, September 2006.
[38] Kwak DY, Tokugawa N, Yoshida K. Flight Test results of NEXST-1 airplane. In: Proceedings of international workshops on numerical simulation technology

for design of next generation supersonic civil transport (SST-CFD workshop), JAXA-SP-06-029E, 2007, p. 538–46.
[39] Yoshida K. Outline of CFD workshop on flight test results of NEXST-1 airplane. In: Proceedings of international workshops on numerical simulation technology for design of next generation supersonic civil transport (SST-CFD workshop), JAXA-SP-06-029E, 2007, p. 547–51.
[40] Yoshida K. Summary of CFD workshop on NEXST-1 flight test. In: Proceedings of international workshops on numerical simulation technology for design of next generation supersonic civil transport (SST-CFD workshop), JAXA-SP-06-029E, 2007, p. 688–96.
[41] Yoshida K. Aerodynamic design of the NEXST-1 airplane. Concluding Report of Flight Test Data Analysis on the Supersonic Experimental Airplane (NEXST-1), JAXA-SP-08-008, 2008, p. 45–72 [in Japanese].
[42] Kwak DY, Yoshida K, Ishikawa H, Noguchi M. Flight test measurements of surface pressure on unmanned scaled supersonic experimental airplane. AIAA-2006-3483, 2006.
[43] Tokugawa N, Yoshida K. Transition detection on supersonic natural laminar wing in the flight. AIAA-2006-3165, 2006.
[44] Tokugawa N, Kwak DY, Yoshida K. Transition measurement system of experimental supersonic transport—NEXST-1. ICAS2006-6.2.1, 25th ICAS, Hamburg, September 2006.
[45] Tokugawa N, Kwak DY, Yoshida K, Ueda Y. Transition measurement of natural laminar flow wing on supersonic experimental airplane NEXST-1. Journal of Aircraft 2008;45(5):1495–504.
[46] Makino Y, Iwamiya T, Lei Z. Fuselage shape optimization of a wing-body configuration with nacelles. Journal of Aircraft 2003;40(2):297–302 [or AIAA-2001-2447, 2001].
[47] Zhong L, Makino Y, Iwamiya T. Nacelle Design study of a supersonic experimental airplane using aerodynamic shape optimization. AIAA 2002-0105, 2002.
[48] Murakami A, Watanabe Y, Fujiwara H. Air-intake aerodynamic design for NAL's scaled supersonic jet-powered experimental airplane. In: Proceedings of 2001 meeting of Japan Society of Fluid Mechanics, 2001, p. 559–60 [in Japanese].
[49] Fujiwara H, Murakami A, Watanabe Y. Numerical analysis on shock oscillation of two-dimensional external compression intakes. AIAA 2002-2740, 2002.
[50] Watanabe Y, Murakami A, Fujiwara H. Effect of sidewall configurations on the aerodynamic performance of supersonic air-intake. AIAA-2002-3777, 2002.
[51] Watanabe Y, Murakami A. Control of supersonic inlet with variable ramp. ICAS 2006, 2006.
[52] Akastuka J, Watanabe Y, Murakami A, Honami S. Porous bleed model for boundary condition. AIAA-2006-3682, 2006.
[53] Shimbo Y, Makino Y, Noguchi M. Wind tunnel test of the powered national supersonic experimental transport. In: Proceedings of 2001 meeting of Japan Society of Fluid Mechanics, 2001, p. 557–8 [in Japanese].
[54] Yoshida K, Noguchi M, Shimbo Y, Kuroda F. Comparison of wind tunnel test and CFD analysis on an airframe/nacelle configuration of the scaled supersonic experimental airplane. In: Proceedings of the 39th aircraft symposium, no. 3D15, 2001 [in Japanese].
[55] Shimbo Y, Noguchi M, Makino Y. Blowdown tunnel application of pressure sensitive paint. AIAA-99-3169, 1999.
[56] Makino Y, Suzuki K, Noguchi M, Yoshida K. Nonaxisymmetrical fuselage shape modification for drag reduction of low-sonic-boom airplane. AIAA Journal 2003;41(8):1413–20 [or AIAA-2003-557, 2003].
[57] Makino Y. Low sonic-boom design of a Silent supersonic technology demonstrator—development of CAPAS and its application. In: Proceedings of international workshops on numerical simulation technology for design of next generation supersonic civil transport (SST-CFD workshop), JAXA-SP-06-029E, 2007, pp. 697–704.